防止彎曲漏光之可撓式背光設計與製作

碩士研究生：林姚順　　指導教授：謝漢萍 教授

黃乙白 副教授

國立交通大學　　顯示科技研究所

摘　要

在顯示器的應用中，輕薄短小和可攜帶性的特性將會使可撓式顯示器成為未來的趨勢。作為一種成熟的技術，液晶顯示器有很高的潛力發展可撓式顯示器。然而，穿透式的液晶顯示器需要背光源才能發揮效用。現有的幾種可撓式背光技術中，正面臨著均勻度或效率過低的問題。

本論文提出一藉由防止彎曲漏光以維持均勻度的可撓式背光。利用拋物線全反射鏡，特殊設計的導光板只允許光傳播方向平行於彎曲軸。導光板中的參數，包含拋物線全反射鏡和 V 型微結構，藉由模擬軟體進行優化。為了驗證概念，以雷術切割和鑽石刀加工製做出導光板模型。實驗結果證明，導光板分別在平坦和彎曲的狀態下，垂直導光板方向的一維均勻度皆能維持在 80%以上，其中彎曲曲率半徑可以達到 5 公分。並且在平坦和彎曲的情況下，亮度差異(誤差函數)小於 10%。此外，應用外部螢光粉技術所造成均勻的角分佈，也使得在真實情況中，人眼所察覺的亮度空間分佈一樣是均勻的。因此，本防止彎曲漏光之可撓式背光，有潛力可以應用在可撓式液晶顯示器上。

Design and Fabrication of Flexible Backlight with Bending-loss Prevention

Master Student: Yao-Shun Lin **Advisors: Dr. Han-Ping D. Hsieh**
Dr. Yi-Pai Huang

Display Institute

National Chiao Tung University

Abstract

In display applications, flexibility will be a trend in the future due to the features like compactness and portability. As a mature technology, LCD has the potential for development in flexible display. However, the transmissive LCD requires the backlight for operation. Nowadays, several kinds of flexible backlight suffer from low luminance uniformity or low optical efficiency.

In this thesis, the flexible backlight was proposed to maintain the luminance uniformity by bending-loss prevention. The light guide is designed to permit light propagating parallel to bending axis by parabolic TIR reflector. The parameters of light guide, including the parabolic TIR reflector and the v-cut out-coupler, were optimized by optical simulation tool. The prototype of light guide was fabricated by laser cutting and diamond turning to verify the concept. From the experimental results, the 1D uniformity from the normal of light guide could successfully kept over 80% in both flat case and bending case, which the radius of curvature could reach 50mm. Additionally, the luminance difference (error function) between in flat case and

bending case is lower than 10%. Moreover, the luminance angular profile applied remote phosphor technology is uniform so that the luminance spatial profile in real case perceived by human eyes is also uniform. Therefore, the flexible backlight with bend-loss prevention has the potential to be applied in flexible LCD.

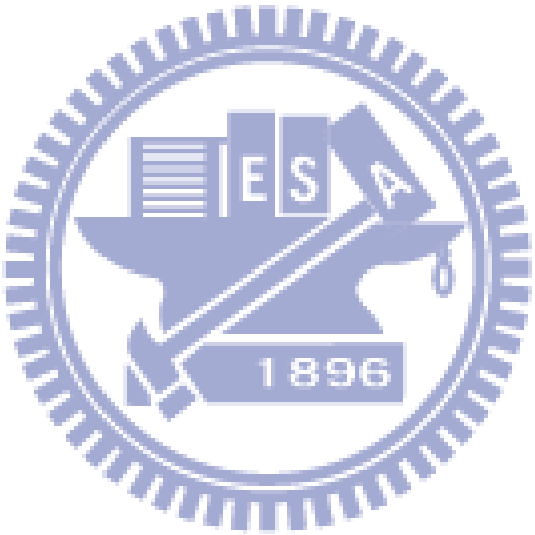

誌　謝

首先要感謝的是謝漢萍老師與黃乙白老師，在我碩班過程中予我的指導與訓練，包括研究的邏輯思考與組織報告的能力，以及提供良好的研究環境與資源，讓我順利完成論文，獲益良多。

也感謝口試委員們在百忙之中蒞臨，並且不吝嗇地提出寶貴的建議，補足我思考上遺漏的地方。感謝洪健翔學長在研究上細心的指導與協助，在無數次的討論過程中給予我許多實用的意見。實作方面，感謝工研院機械所李企桓博士與林宗信先生的協力與幫忙。

實驗室的生活多采多姿，留下許多難忘的回憶。感謝芳正學長、喬舜學長、均合學長、韻竹學姐、凌嶢學長、國振學長、柏全學長、奕智學長及精益學長的照顧，還有相同研究領域的靖堯、博文、浩彣以及秉彥的切磋。一群同甘共苦的同學們，怡菁、期竹、景文、世勛、耆賢、泳材、甫奕以及光電三俠一起學習與成長的過程，更是我珍貴的回憶。有育誠、致維等其他學長姐和學弟妹們在課業與生活上的陪伴，研究上的辛苦與煩悶隨著歡笑聲而煙消雲散。另外，也感謝實驗室的助理們，為我們學生處理許多重要的事情。

謝謝交大棒球隊的黃杉楹教練和隊友們，交大電物的同學、學長姐和學弟妹們，系棒的隊友們，因為有你們，豐富了我的生活。

最後感謝家人的支持與鼓勵，讓我無後顧之憂地完成學業。在此致上我最誠摯的感謝。

Table of Contents

Figure Captions

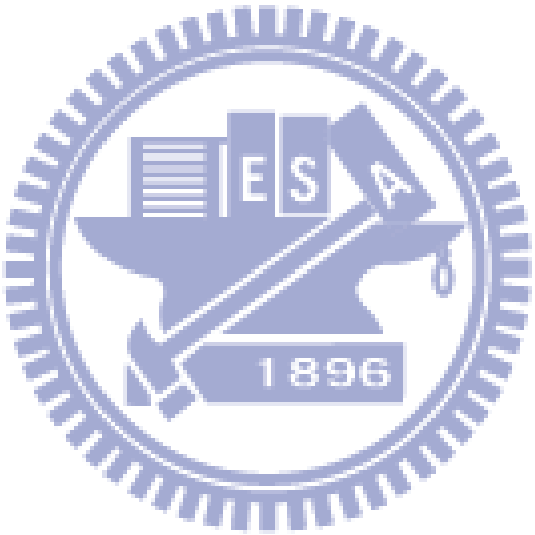

List of Tables

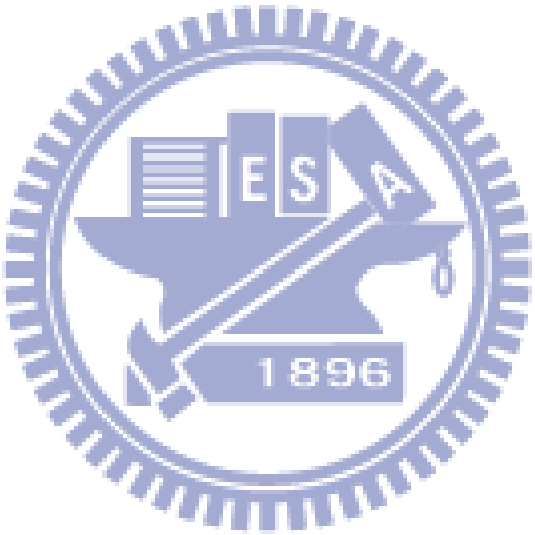

Chapter 1

Introduction

The development of display technology has attracted great attention and made remarkable progress in recent years. Flat panel displays can be generally classified according to radiating methods, which are emissive and passive displays. Emissive displays include the organic light emitting diode (OLED), the plasma display panel (PDP), and the field emitting display (FED) [1][2][3]. However, the most popular flat panel display is one of the passive displays, liquid crystal display (LCD) [4]. In the several applications, the flexibility of information displays is a new subject because of the requirement of the paper-like display, which is expected to replace the traditional papers for the purpose of environmental protection.

1.1 Flexible display

Since flexible display requires paper-like configuration, such displays have several important features, including compactness, bending capability, and portability. Because of these features, the flexible displays are suitable for many applications such as a wearable display, a smart card, a personal information assistant, and an electronic book. There have been many available display technologies having the capability to be used as a flexible display. Examples include the OLED, the electrophoretic display (EPD), the electrochromic displays (ECD), and the Cholesteric liquid crystal (ChLCD), as shown in Fig. 1-1 Flexible display applications.[5][6][7]. These display technologies still have numerous issues like short lifetime, weak color, high driven

voltage, long response time, and high power consumption. Thus, transmissive LCDs, which have well-developed quality, have the potential for flexible display. A significant amount of research has been done on developing curved LCDs, using bendable substrates, with some success[8].

As a transmissive technology, LCDs generally require backlight for operation. When typical constructions of LCD backlights are curved over a certain radius, the uniformity and brightness of the backlight change significantly. This thesis presents a new backlight system that maintains uniformity and brightness at a range of different curvatures for implementing in flexible LCDs.

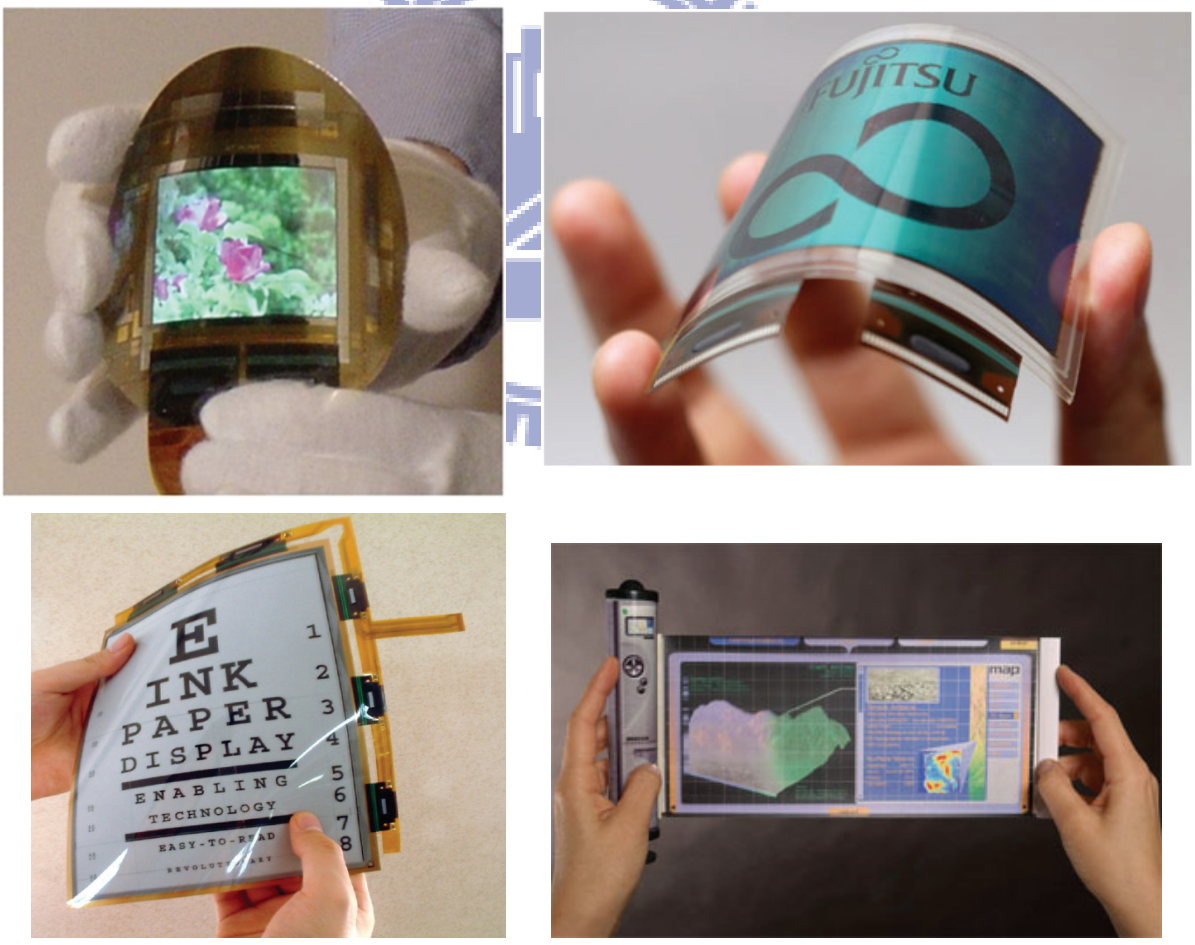

Fig. 1-1 Flexible display applications.

1.2 Side-emitting backlight

Since the LC panel does not emit light by itself, a backlight system is required to provide illumination. In general, backlight systems can be classified into two types according to the location of the light source. These may be cold cathode fluorescent lamps (CCFLs) or light emitting diodes (LEDs). When the light sources are directly behind the LC panel, this is called direct-emitting type. When the light sources are placed at the edge of a light guide plate (LGP), it is called side-emitting type. The direct-emitting backlight, as shown in Fig. 1-2(a), is typically used in large size LCD applications because of its high brightness and efficiency. However, disadvantages of bulk and low uniformity make it unsuitable for mobile products. In the other words, direct-emitting backlight needs space for mixing light to maintain uniformity so it can not be thin and bendable. The side-emitting backlight, as shown in Fig. 1-2(b), is usually applied in mobile products because of slim thickness and light weight. The following are the features of side-emitting backlight. First, side-emitting backlight with fewer LEDs can reduce power consumption for sufficient brightness. Next, the light source position makes the side-emitting backlight slim. Moreover, the out-coupler on light guide plate is utilized to redirect the light for high uniformity. Therefore, side-emitting backlight is more suitable than direct-emitting type for flexible LCDs.

Additionally, remote phosphor technology applied in backlight system will be introduced in the next section.

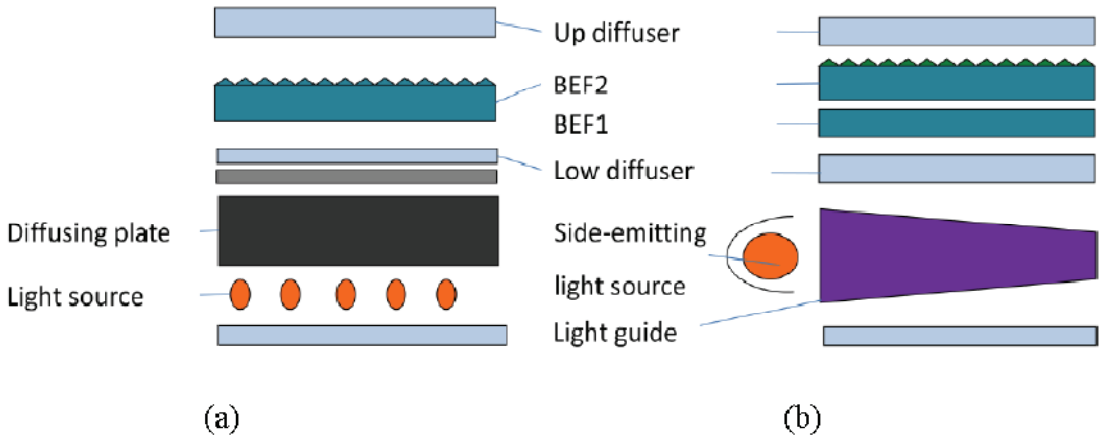

Fig. 1-2 Schematic configuration of the transmissive LCDs of (a) direct-emitting (b) side-emitting backlight system

1.3 Remote phosphor technology

Remote phosphor technology is extensively applied in white LED illumination. It includes point light source and planar light source applications. In point light source application, remote phosphor technology mainly contributes to increase extraction efficiency of LED[9][10][11][12]. Besides, it mainly contributes to increase uniformity in planar light source applications[13][14][15][16].

Remote phosphor technology was firstly developed for LED packaging since Nadarajah's research (2005) [9]. A light-excited illuminating device configuring with external photo-fluorescent structure is so-called remote phosphor technology. Fig. 1-3(a) shows the scheme of the conventional pcLED which utilizes a blue LED chip irradiating Cerium(III)-doped $Y_3Al_5O_{12}$ phosphor[17] (YAG-phosphor) to obtain white light emission. The broadband YAG-phosphor is coated on the LED die surface and packaged inside the device. This configuration has low efficiency because the diffuse phosphor directs 60% of total white light emission back toward the chip and leads losses of energy. Nadarajah *et al.* proposed the scattered photon extraction (SPE)

pcLED[9] which contained a external YAG-phosphor. The external phosphor was coated outside the LED chips as shown in Fig. 1-3(b). Due to the separation of LED die and extraction of backward-emitted rays, the efficiency of SPE pcLED was 61% higher than conventional pcLED.

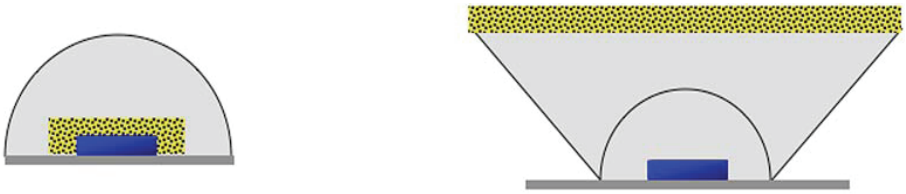

(a) Conventional pcLED

(b) Scattered photon extraction (SPE) pcLED

Fig. 1-3 Schematic configurations of light emitting diodes.

Basing on research of the remote phosphor technology adopted pcLEDs, the side-emitting backlight with remote phosphor technology is utilized in this thesis. Comparing with conventional side-emitting backlight, the configuration with large-sized remote phosphor layers coated on flat substrates is shown in Fig. 1-4.The phosphor layer is placed between light guide and optical films. The light guide can convert point light source into planar light source. The phosphor layer can be excited by blue light and emit yellow light to produce planar white light for backlight. Due to the backward scattering of excited yellow light, the side-emitting backlight with remote phosphor technology has higher optical efficiency and uniformity than conventional side-emitting backlight.

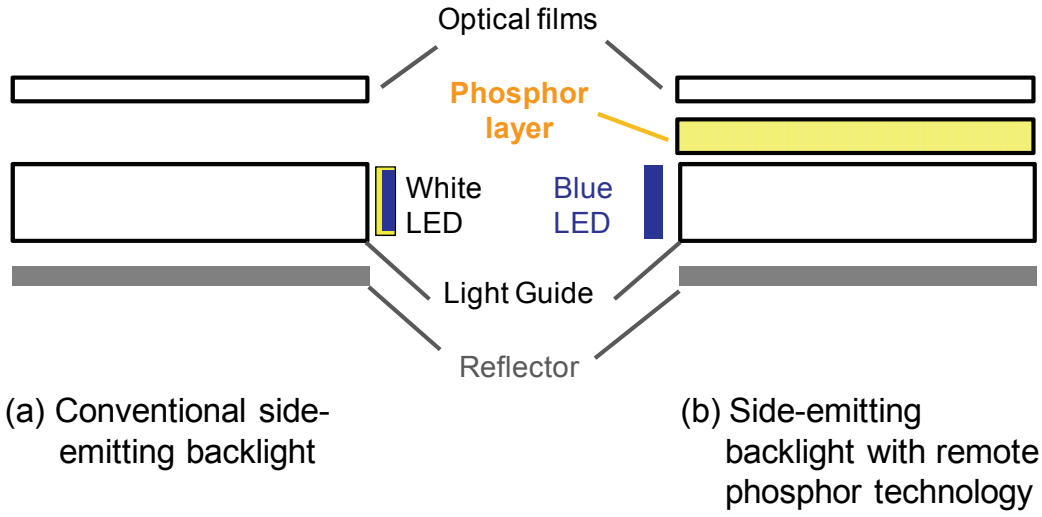

Fig. 1-4 Schematic configuration of (a) conventional side-emitting backlight and (b) side-emitting backlight with remote phosphor technology

1.4 Prior arts: Flexible backlight

The flexible backlight includes a bendable light guide plate and a light source. The following are two kinds of flexible backlight constructions which have been proposed.

(a) Side-emitting type[18]

The backlight where the source is located on the edge of bendable light guide plate is side-emitting type. Light emitted from the light source propagates in the bendable light guide plate through total internal reflection (TIR). The propagating light that strikes the out-coupler at the bottom of light guide plate is diffused, and the diffused light is radiated out of the light guide plate. The advantages of this emission type are light weight, slimness, low cost, and high coupling efficiency from the light source. However, uniformity decreases when backlight is bent. Moreover, the bending direction is limited, only allowing bending in the θ direction, as shown in Fig. 1-5.

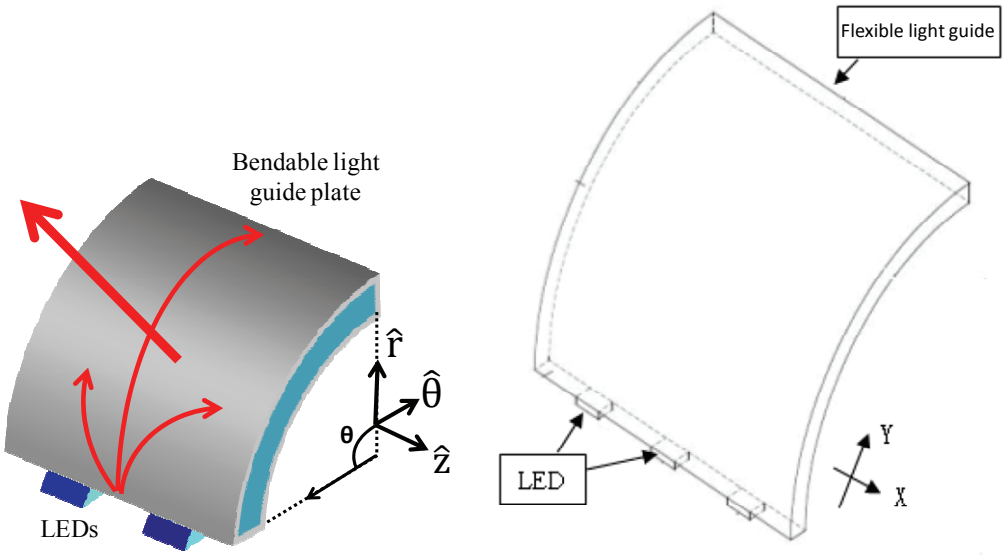

Fig. 1-5 Side-emitting type flexible backlight

(b) Optical fibers arrangement type[19]

Optical fibers arrangement type is when optical fibers are arranged below the bendable light guide plate, as shown in Fig. 1-6. The light propagates in optical fibers through TIR. Then, the TIR is interrupted by v-cut patterns which extract linear light on the bottom of optical fibers. The patterns on the light guide plate, which is above optical fibers, make linear light become uniform planar light. Compared with the side-emitting type, the optical fibers arrangement type has high uniformity when bent and bending direction freedom. Nevertheless, the disadvantages of this type are wide thickness, high cost, and low coupling efficiency between LEDs and optical fibers.

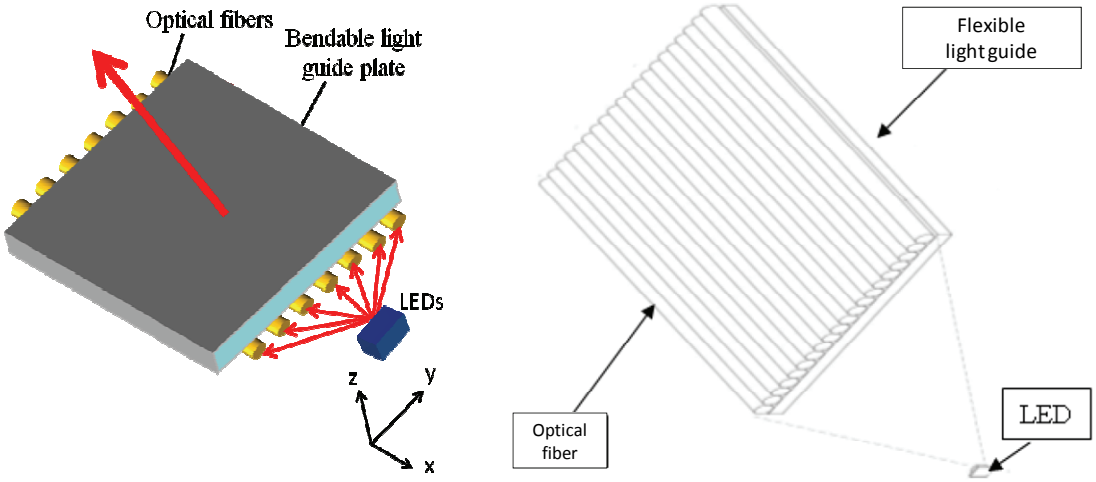

Fig. 1-6 Optical fibers arrangement type flexible backlight

1.5 Motivation and objective

The flexible displays will be a trend in the future. Although some display technologies, like OLED and EPD, can be used as flexible display, there are many problems, like high cost, short lifetime, weak color, and long response time, to be solved. For producing the flexible LCD, the special backlight which can be bent without optical loss is required. Some methods of flexible backlight have been proposed, but they can't reach high uniformity, high efficiency, light weight, and slim thickness simultaneously when backlight is bent. One of the reasons is the bending-loss for causing the non-uniform luminance spatial profile.

In this thesis, the objective is to design a backlight module for flexible display. The size is 3.3 inches, the thickness of light guide is 0.5mm, the uniformity is higher than 70% in both flat and bending case, and the bending ability can reach radius of curvature 50mm. Basing on previous studies of flexible backlight, the construction of flexible backlight with bending-loss prevention was proposed. Simulation model was created for analysis and optimization. Moreover, prototype was fabricated for verification and experiment.

1.6 Organization

This thesis is organized as follows: The principles of backlight systems are presented in **Chapter 2**. In **Chapter 3**, the design concept is described. Practical design case and simulation results are illustrated in **Chapter 4.** In **Chapter 5**, the fabrication methods and results of the prototype are shown, and experimental results are discussed. Finally, conclusions and recommendations for the future work are presented in **Chapter 6**.

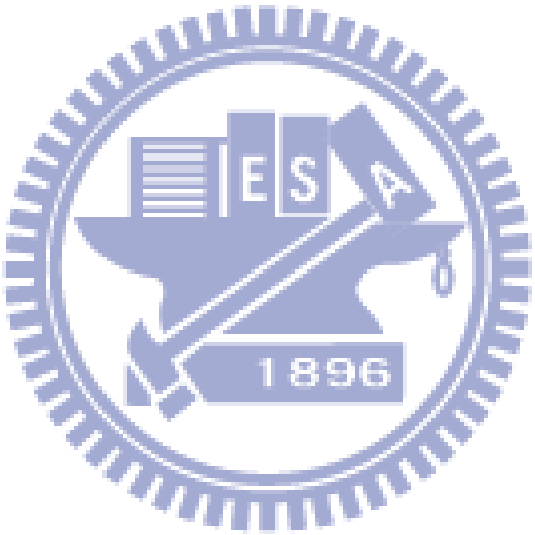

Chapter 2

Optic and Color Principles for Backlight Systems

For the purpose of designing and analyzing backlight systems, several optical principles are described in this chapter. Rays emitted from light source pass through an optical system following the principles of geometrical optics. Ray-tracing results are mainly interpreted by Radiometry and Photometry quantities. Moreover, basing on colorimetry, the CIEXYZ and CIELUV color spaces, which specify color numerically, are also presented to illustrate the characterizations of phosphor films in this chapter.

2.1 Geometrical optics in illumination system

Light is an electromagnetic wave phenomenon. As the wavelength of light is much smaller than surrounding objects it propagates through and around, the behavior of light can be approximated and described by ray optics (geometrical optics). In geometrical optics, light travels in the form of rays and obeys a set of geometrical rules including laws of refraction and reflection.

2.1.1 Laws of refraction and reflection

Law of refraction (Snell's law)

When a light ray is incident on a boundary surface of two media where the refractive indices of the two media are n_i and n_t, the ray is split into a reflected ray and a refracted (transmitted) ray as shown in Fig. 2-1. The incident ray, the normal direction of the surface, and the refracted ray all lie in the same plane called incident plane. The

propagating direction of the refracted ray follows the relationship,

$$n_i \sin\theta_i = n_t \sin\theta_t, \tag{2.1}$$

where θ_i is the angle between the incident ray and the normal direction of the surface (the incidence angle) and θ_t is the angle between the refracted ray and the surface normal (the refraction angle). This relationship is called Snell's law and can be proved by Fermat's Principle[20].

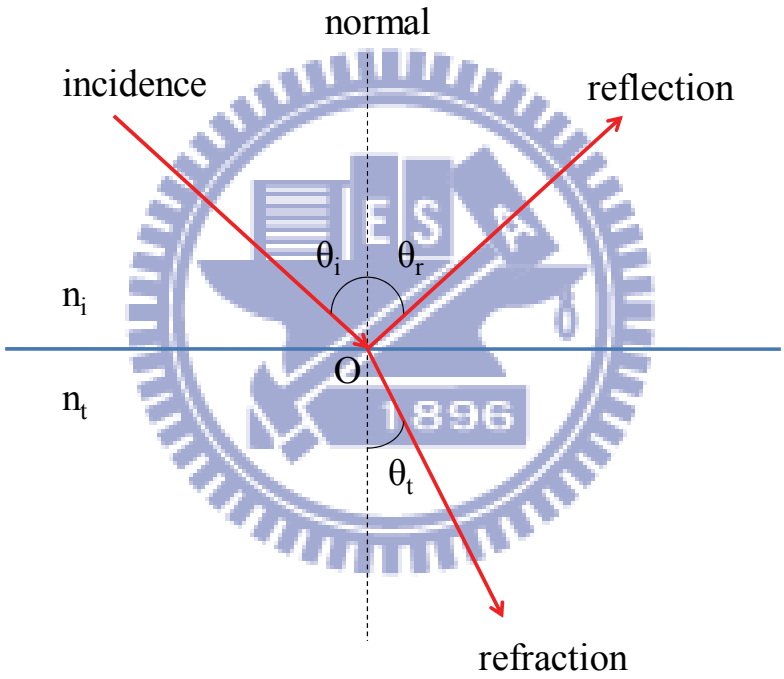

Fig. 2-1 Reflection and Refraction on a boundary surface

Law of reflection

The reflected light lies in the incident plane and possesses an angle θ_r with respect to the normal direction of the surface. The angle of reflection is equal to the angle of incidence,

$$\theta_i = \theta_r, \tag{2.2}$$

which is called the law of reflection.

Therefore, the propagating direction of a light ray in an optical system can be traced and calculated.

2.1.2 **Parabola reflector**

Reflectors are extensively applied in illumination system. The most popular examples include free-form, ellipse, hyperbola, and parabola reflector. The shape of free-form reflector is designed for special purpose[21]. It is generated by solving several differential equations numerically, which give a collection of points on the surface or curve, as shown in Fig. 2-2. In mathematics, ellipse, hyperbola, and parabola are curves obtained by intersecting a cone with a plane, as shown in Fig. 2-3. The circle and the ellipse arise when the intersection of cone and plane is a closed curve. The circle is obtained when the cutting plane is parallel to the plane of the generating circle of the cone. Additionally, the plane intersects both halves of the cone, producing two separate unbounded curves, which is a hyperbola. Besides, if the cutting plane is parallel to exactly one generating line of the cone, then the conic is unbounded and is called a parabola.

In parabola, if any line $\overline{SP}$, which is parallel to the axis of symmetry L, is reflected by parabola, the reflected line $\overline{PF}$ will pass through the focus F, as shown in Fig. 2-4. A parabolic reflector is a reflective device used to collect energy such as light, sound, or radio waves. Since the principles of reflection are reversible, parabolic reflectors can also be used to project energy of a source at its focus outward in a parallel beam, used in devices such as spotlights and car headlights.

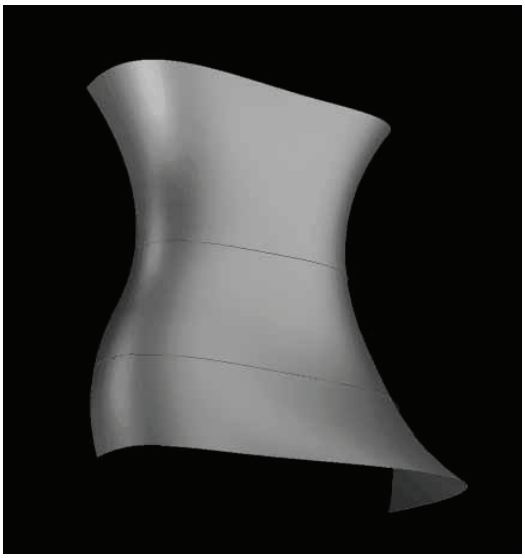

Fig. 2-2 Free-form surface reflector [http://en.wikipedia.org/wiki/Conic_section]

Fig. 2-3 Types of conic sections: (a) Circle and ellipse (b) Hyperbola (c) Parabola [http://en.wikipedia.org/wiki/Parabolic_reflector]

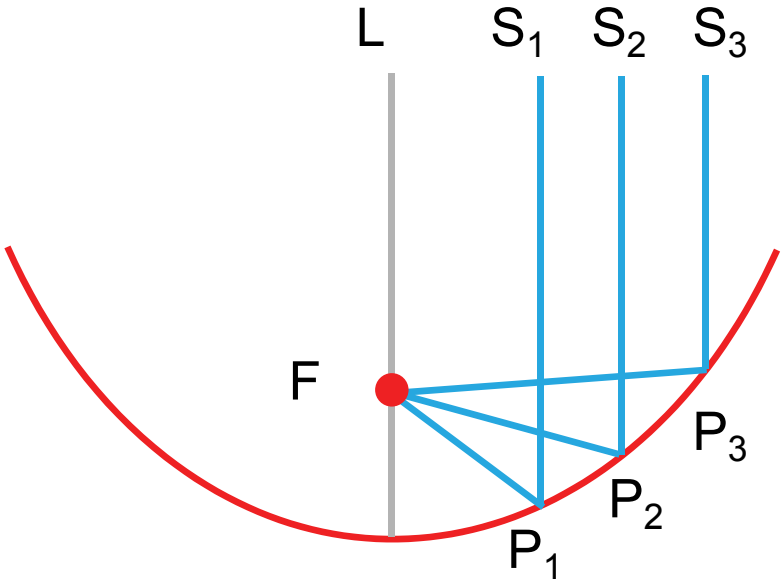

Fig. 2-4 Property of parabola

2.2 Radiometry and Photometry quantities

2.2.1 Radiometry

Radiometry is the science of measurement of electromagnetic radiation. Some fundamental quantities which characterize the energy content of radiation are summarized in Table 2-1[22].

Table 2-1 Energy-based units

Quantity	Symbol	Definition	SI Units
Radiant energy	Q_e	--	Joule
Radiant flux	Φ_e	dQ_e/dt	Watt
Radiant exitance	M_e	$d\Phi_e/dA$	$Watt/m^2$
Irradiance	E_e	$d\Phi_e/dA$	$Watt/m^2$
Radiant intensity	I_e	$d\Phi_e/d\Omega$	Watt/sr
Radiance	L_e	$dI_e/dA_\perp$	$Watt/sr \cdot m^2$

From the above table, Q_e is the energy of a collection of photons while the energy of a single photon is hv. Radiant exitance M_e pertains to radiation leaving a surface; Irradiance E_e pertains to radiation incident on a surface. Radiant intensity I_e is the radiant flux Φ_e emitted per unit of solid angle Ω by a point source in a given direction. The Radiance L_e indicates the radiant intensity per unit of projected area perpendicular to the light of sight as shown in Fig. 2-5.

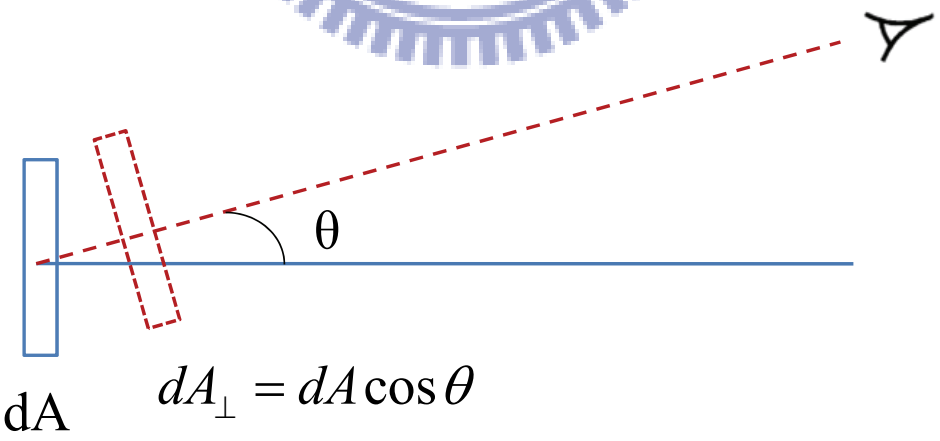

Fig. 2-5 Definition of projected area

2.2.2 Photometry

Compared to Radiometry that measures all radiant energy, Photometry applies only to the visible portion of the optical spectrum for the human eye. Since the human eye does not respond with equal sensitivity at all wavelengths of visible light, the radiant power at each wavelength is weighted by CIE luminous efficiency curve which models human brightness sensitivity. The standard model that represents response or sensation of brightness for the eye versus wavelength is reproduced in Fig. 2-6.

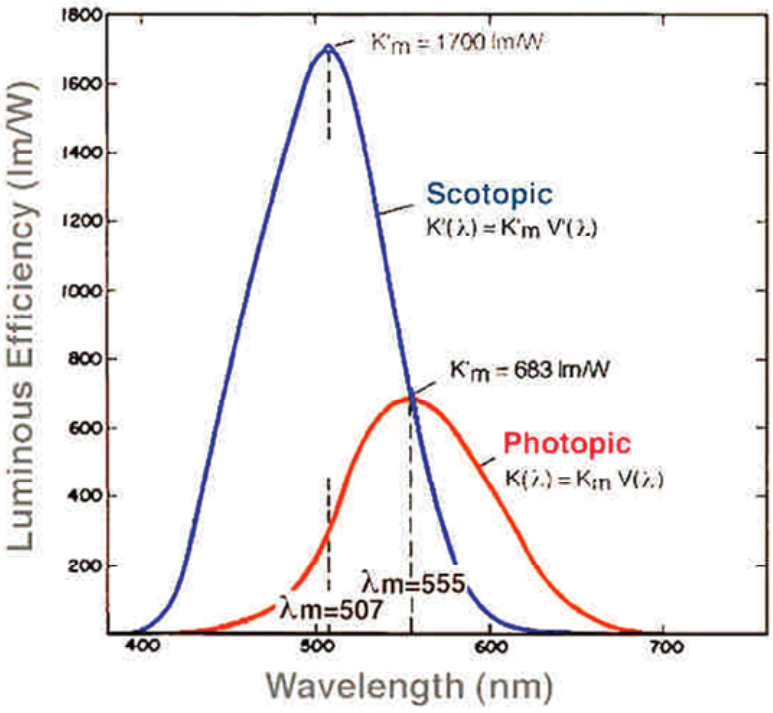

Fig. 2-6 Scotopic and Photopic spectral sensitivities

Photometric quantities are related to Radiometric quantities through the luminous efficiency curve. One watt of radiant energy at the w6avelength of maximum visual sensitivity (555 nm) is defined to be 683 lumens. Thus, the luminous flux emitted from a source with a radiant flux $\Phi_\lambda(\lambda)$ is given by

$$\Phi_v(\lambda) = 683 \text{ lm/w} \cdot \int V_\lambda(\lambda)\Phi_\lambda(\lambda)d\lambda \tag{2.3}$$

where $\int V_\lambda(\lambda)$ is the normalized Luminous efficiency depicted in Fig. 2-7. Some Photometric units parallel to stated Radiometric units are illustrated in Table 2-2.

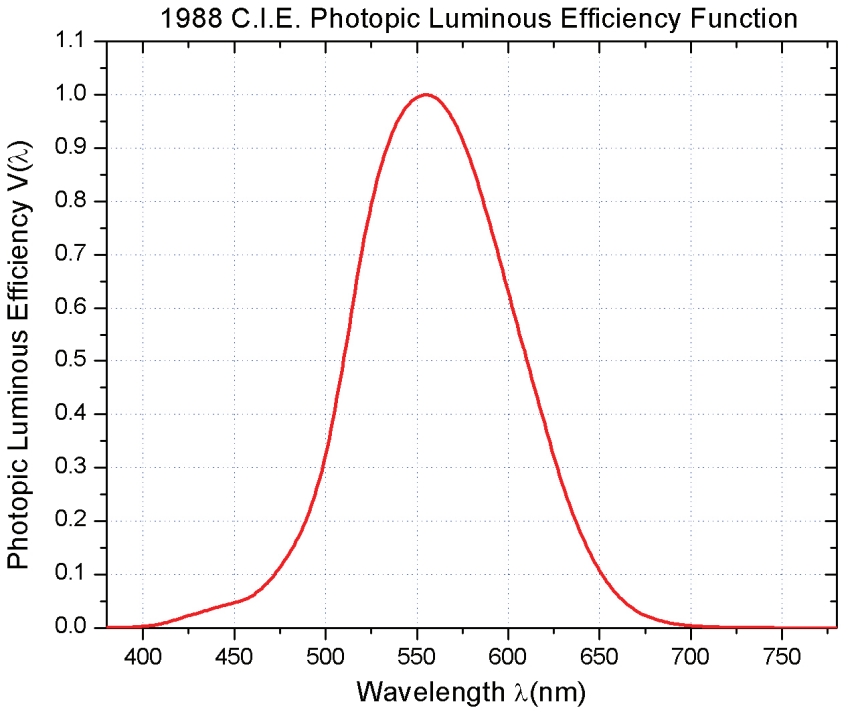

Fig. 2-7 1988 CIE Photopic Luminous Efficiency Function

[http://note.j-i-n.name/2005/06/photopic-luminous-efficiency-function]

Table 2-2 Photon-based Units

Quantity	Symbol	Definition	SI Units
Luminous energy	Q_v	--	lumen • s
Luminous flux	Φ_v	dQ_v/dt	lumen (lm)
Luminous exitance	M_v	$d\Phi_v/dA$	lumen /m^2
Illuminance	E_v	$d\Phi_v/dA$	lumen /m^2 or lux
Luminous intensity	I_v	$d\Phi_v/d\Omega$	lumen /sr or candela
Luminance	L_v	$dI_v/dA_\perp$	lumen/sr • m^2 or nits

2.3 Colorimetry

Colorimetry is the science relating color comparison and matching. As mentioned earlier, for visible light, the optical radiations within wavelengths ranging from 380 nm to 780 nm, the photometric quantities have provided measures to describe the amount of energy. However, in human visual system, the optical radiations arouse not only intensity response (brightness) but also chromatic response (chromaticity). Therefore, in this thesis, colorimetry is imported to specify the chromatic performance of backlight units. The CIEXYZ and CIELUV color spaces, which have been developed for denoting colors numerically, are described in the following paragraphs.

CIEXYZ color space

The CIE XYZ system, created by the International Commission on Illuminance (CIE) in 1931, is one of the first mathematically defined color systems that specify colors numerically[23]. The human eye has receptors for short (S), middle (M), and long (L) wavelengths. Thus in principle, three parameters describe a color sensation. The tristimulus values of a color are the amounts of three primary colors in a

three-component additive color model needed to match that test color[24]. In the CIE XYZ system, the tristimulus values are called X, Y, and Z. The tristimulus values for a color with a stimulus $\Psi(\lambda)$ can be derived from the color matching functions, the numerical description of the chromatic response of standard observer[25] (see Fig. 2-8), according to the following equations:

$$X = k\int_{vis} \Psi(\lambda)\bar{x}(\lambda)d\lambda \tag{2.4}$$

$$Y = k\int_{vis} \Psi(\lambda)\bar{y}(\lambda)d\lambda \tag{2.5}$$

$$Z = k\int_{vis} \Psi(\lambda)\bar{z}(\lambda)d\lambda \tag{2.6}$$

where *k* is a constant and the integral is taken in the visible light wavelength. The $\bar{y}(\lambda)$ is set so that is identical to the spectral luminous efficiency function *V(λ)* mentioned earlier. Thus the tristimulus value Y directly expresses a photometric quantity.

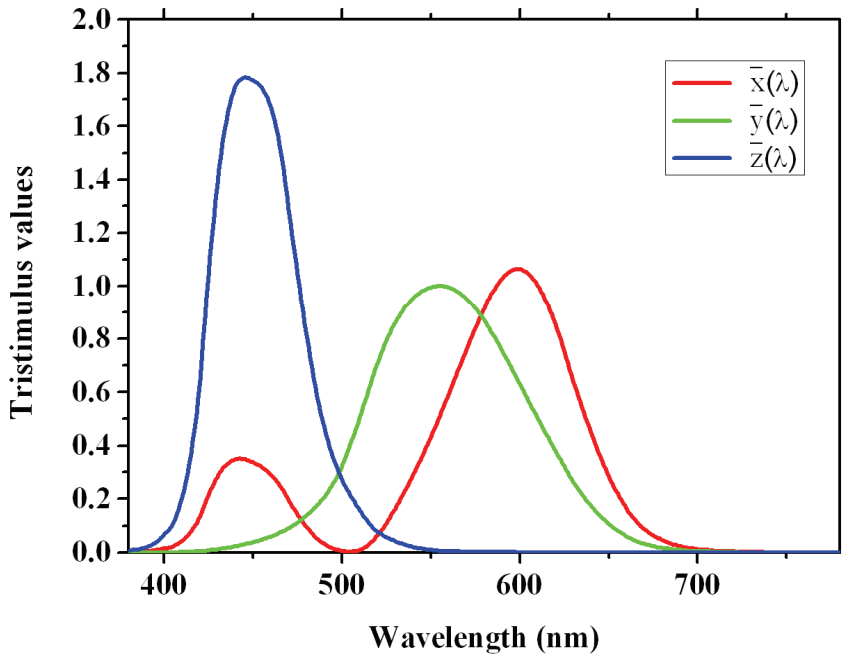

Fig. 2-8 Color matching functions $\bar{x}(\lambda)$, $\bar{y}(\lambda)$, and $\bar{z}(\lambda)$ in the CIE XYZ color system.

Basing on CIE XYZ system, a color could be specified by utilizing the tristimulus values X, Y, and Z in a three-dimensional color space, called CIEXYZ color space. Besides, for convenient descriptions of colors, a color space specified by x, y, and Y, known as CIExyY color space, was derived[26] The x and y are defined as following equations:

$$x = \frac{X}{X + Y + Z} \tag{2.7}$$

$$y = \frac{Y}{X + Y + Z} \tag{2.8}$$

$$z = \frac{Z}{X + Y + Z} = 1 - x - y \tag{2.9}$$

The z coordinate could be omitted by providing Y parameters which is a measure of the luminance of a color. Accordingly, the chromaticity description of a color could be expressed more conveniently in a two-dimensional plane, which is called CIE xy chromaticity diagram and be widely used in practice (see Fig. 2-9).

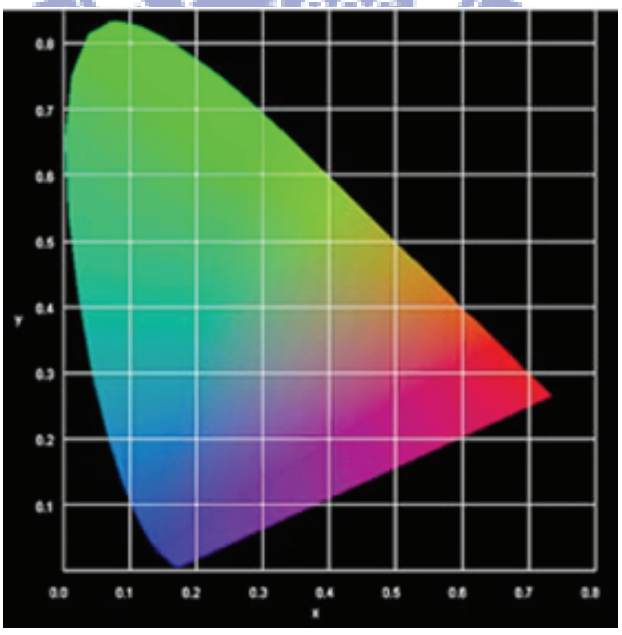

Fig. 2-9 xy chromaticity diagram of CIE XYZ color system.

However, the *xy* chromaticity diagram is highly non-uniform and has been found to be a serious problem in practice[27]. The color difference between two colors could not be calculated by using CIEXYZ color space or *xy* chromaticity diagram. Therefore, a uniform color space, the CIELUV color space, is proposed to replace the non-uniform CIEXYZ color space.

CIELUV color space

The CIELUV color space adopted by CIE in 1976 is an attempt to define an encoding with uniformity in the perceptibility of color difference[28]. Such a uniform color space is based on a simple-to-compute transformation of the 1931 CIEXYZ color space[29][30]. For the non-linear relations from CIEXYZ color space to CIELUV color space, the three-dimensinal orthogonal coordinates adopted in CIELUV color space are defined as follows[31]:

$$L^* = 116(Y / Y_n)^{1/3} - 16 \tag{2.10}$$

$$u^* = 13L^*(u' - u_n') \tag{2.11}$$

$$v^* = 13L^*(v' - v_n') \tag{2.12}$$

where *u'* and *v'* is the coordinates of two-dimensional *u'v'* chromaticity diagram (Fig. 2-10) defined as Equation 2.13 and 2.14, Y_n, u_n', and v_n' are the tristimulus value and the chromaticity coordinates *u'* and *v'* of reference white, respectively.

$$u' = \frac{4X}{4X + 15Y + 3Z} \tag{2.13}$$

$$v' = \frac{9Y}{X + 15Y + 3Z} \tag{2.14}$$

Basing on the uniform CIELUV color space, the color difference of two colors could be calculated. The color difference $u'v'$ between two colors (u_1',v_1') and (u_2',v_2') at the *u'v'* chromaticity diagram is defined as

$$\Delta u'v' = \sqrt{(\Delta u')^2 + (\Delta v')^2} = \sqrt{(u_1' - u_2')^2 + (v_1' - v_2')^2} \quad (2.15)$$

In this thesis, Equation 2.15 is imported to judge the chromatic performance of the backlight units.

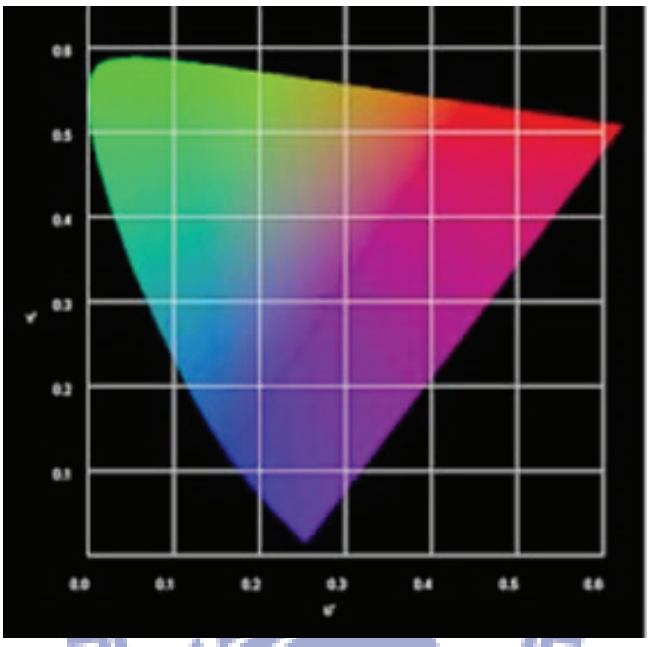

Fig. 2-10 *u'v'* chromaticity diagram of the CIELUV color system.

Chapter 3

Concept of Bending-loss Prevention

The concept of bending-loss and how to prevent bending-loss are described in this chapter. Bending-loss means the light leakage which is caused by curved deformation of light guide, as shown in Fig. 3-1. In general, the light leakage degrades the uniformity of planar light. To prevent bending-loss, the light guide is designed to permit light propagating merely perpendicular to bending direction, as shown in Fig. 3-2.

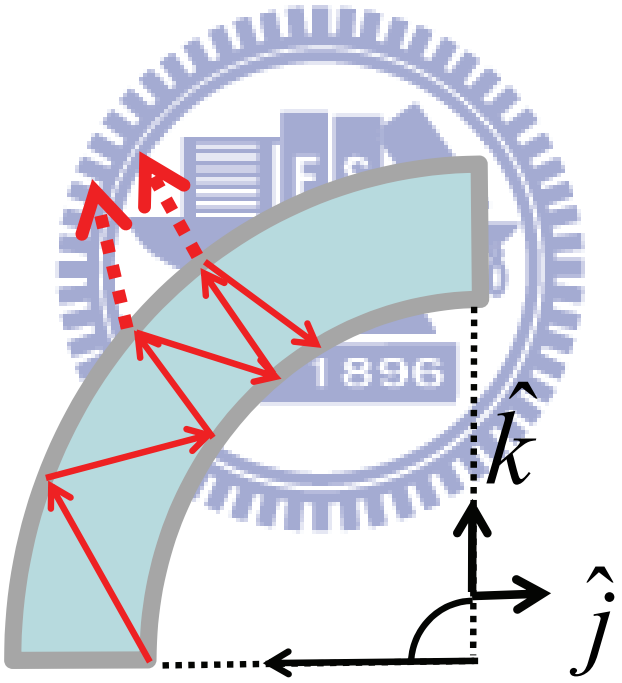

Fig. 3-1 The cause of bending-loss

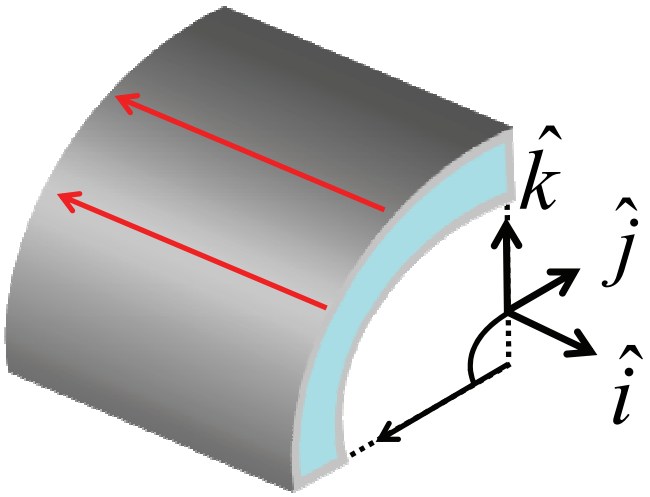

Fig. 3-2 The light guide designed to only permit light propagation component which is perpendicular to bending direction.

3.1 Bending-loss of light guide

Bending-loss results from the curved deformation of light guide, as shown in Fig. 3-1. Therefore, if light guide is flat, the light propagates through TIR in light guide without bending-loss (shown in

Fig. 3-3). When light guide is bent, as shown in Fig. 3-4, light propagation vector can be separated into two components, $\overrightarrow{S_1}$ and $\overrightarrow{S_2}$ which

$$\overrightarrow{S_1} = b\hat{\jmath} + c\,\hat{k} \tag{3.1}$$

$$\overrightarrow{S_2} = a\,\hat{\imath} + c\,\hat{k} \tag{3.1}$$

where a, b, and c are arbitrary constants, and $\hat{\imath}$, $\hat{\jmath}$, and $\hat{k}$ are components of width, length, and thickness of light guide, as shown in Fig. 3-5.

In $\overrightarrow{S_1}$ component, the variation of incident angle θ_i is attributed to the change of geometric shape in light guide. Different bending degree of light guide affects incident angle θ_i. In this case, light leakage occurs with the incident angle θ_i smaller than TIR angle θ_c. The out-coupled and leakage light increase illuminance locally

where the light is emitted out of light guide, and decreases gradually far away from the region. Consequently, this gives rise to reduction in uniformity of planar light.

To maintain high uniformity, the density distribution of out-coupler can be changed according to the amount of light leakage. However, bending-loss for various wavelengths and bending parameters (such as radius of curvature) is different. Thus, it is hard to find the density distribution of out-coupler applicable for various radius of curvature.

In this thesis, the method is proposed to prevent bending-loss by avoiding the light propagating in $\hat{j}$ component. In the other words, $\overrightarrow{S_2}$ with only $\hat{\imath}$ and $\hat{k}$ components is beneficial to prevent bending-loss for any radius of curvature. The design of light guide making the incident light with only $\overrightarrow{S_2}$ component is demonstrated in the following section.

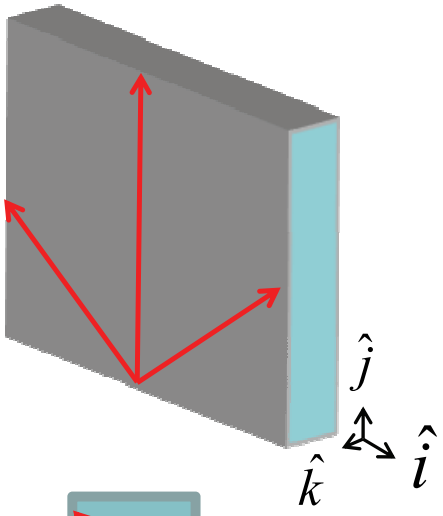

Fig. 3-3 Light propagates through TIR in flat light guide

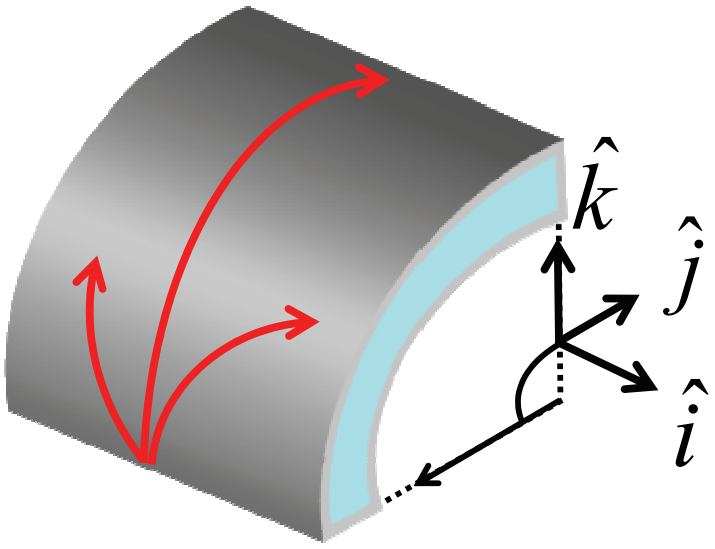

Fig. 3-4 Light propagates in bent light guide

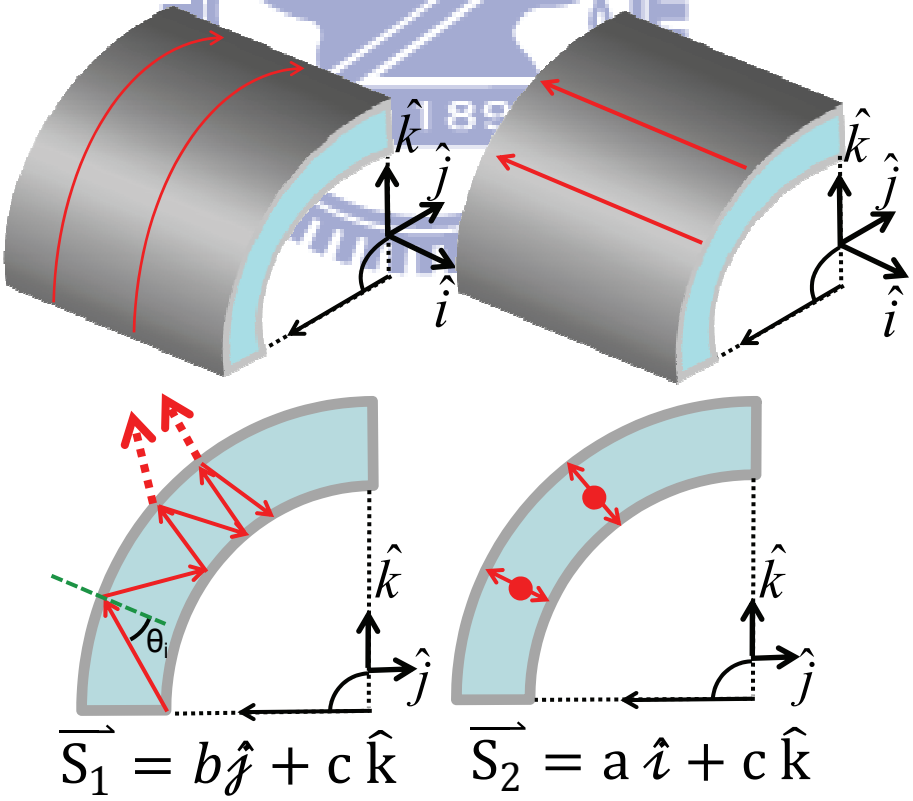

Fig. 3-5 Two separated components of light propagation vector in bent light guide

3.2 Configuration of bending-loss prevention

To obtain collimated light for bending-loss prevention, the parabolic patterns of light guide are utilized. The configuration of proposed flexible backlight with bending-loss prevention is shown in Fig. 3-6. One side of light guide is cut into parabolic pattern array. Blue LEDs are placed adjacent to the associated parabolic patterns respectively. Blue light of point light source emitted from the focus toward $\hat{\jmath}$ component is reflected through TIR by parabolic pattern in a linear parallel ray toward -$\hat{\imath}$ component. Therefore, the light guide without bending-loss can be achieved no matter how bent it is. Besides, the optimized out-coupler at the bottom of light guide can break TIR to redirect the linear light for high planar uniformity in spatial profile. The reflectors located above and below the light guide can reduce light leakage and increase efficiency. The phosphor layer is employed to emit yellow light, as a result, planar white light can be produced. In addition to the generation of planar white light, the backward scattering of excited yellow light can also increase the uniformity of planar light. Fig. 3-7 illustrates the light propagation of resulting $\overrightarrow{S_2}$ component with the bent configuration described as above.

Among these elements, the parabolic pattern and the out-coupler are the key factors to produce the collimated and uniform planar light. Thus, the optimization of parameters for parabolic patterns and out-coupler are investigated in the next chapter.

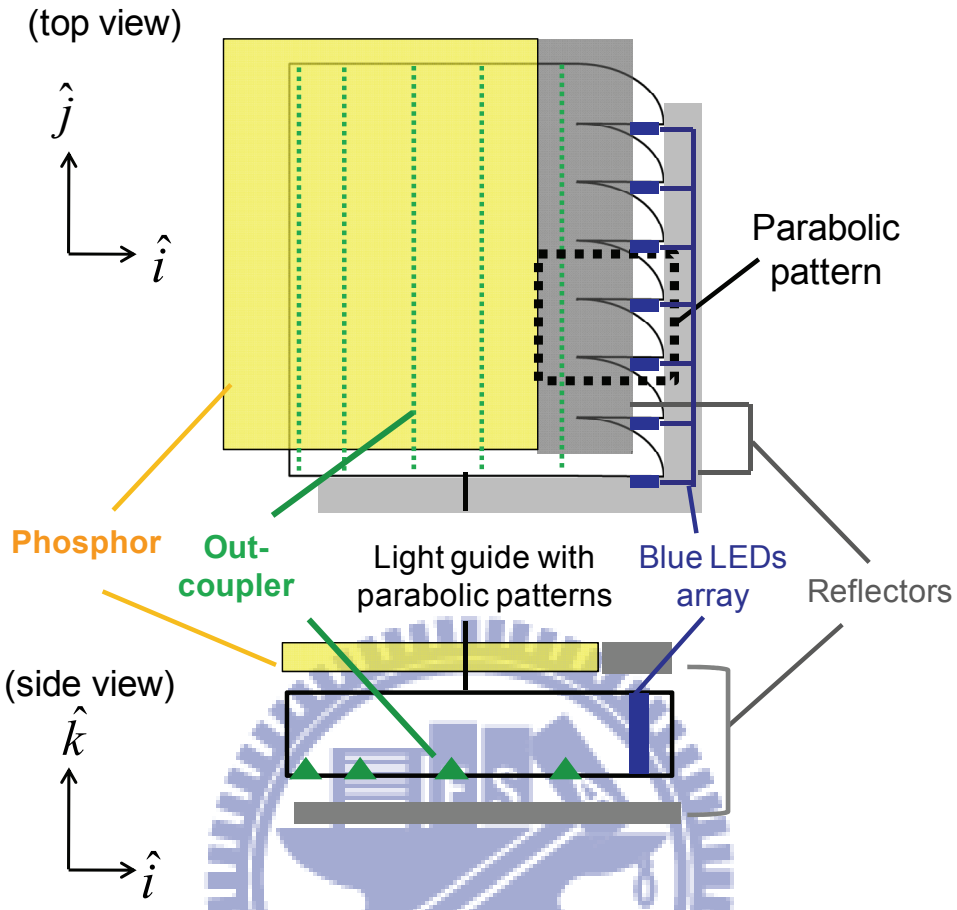

Fig. 3-6 Configuration of bending-loss prevention

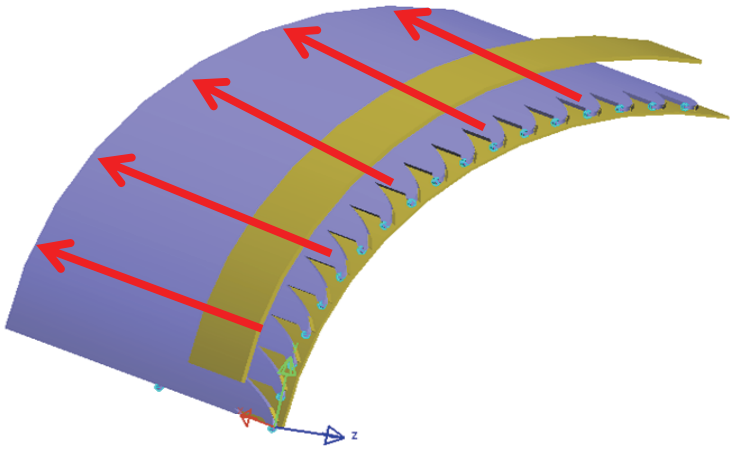

Fig. 3-7 The light propagation with bent configuration

Chapter 4

Simulation and analysis

The simulation results and analyses are described in this chapter. Geometrical parameters, including parabolic TIR reflector and out-coupler, are optimized by simulation software, LightTools. The parabolic TIR reflector of light guide is designed for collimated and uniform linear light. Besides, the out-coupler is used to break TIR in light guide for the luminance angular profile toward the normal of light guide and uniform planar light.

4.1 Parabolic TIR reflector

The purpose of parabolic TIR reflector of light guide is to generate collimated and uniform linear light. Point light source is placed at focus of parabola. Light emitted from the focus is reflected by parabolic TIR reflector, resulting in a parallel linear ray.

However, LED is not an ideal point source. As a result, the light component of the source, which is not emitted exactly from the focus, lead to stray light which affects both collimation and uniformity. Hence, simulation result, including luminance angular profile and luminous exitance spatial profile on the exit surface of the parabolic TIR reflector, are analyzed in the following parts.

4.1.1 Luminance angular profile

The simulation result shows that the LED size more approximative an ideal point source contributes to higher collimated luminance angular profile on the exit surface

of the parabolic TIR reflector. To quantify the LED size, the value of c/w is defined, where c is the focal length of parabola and w is the width of LED, as shown in Fig. 4-1. High value of c/w means that LED approaches an ideal point source. In other words, less stray light not emitted from the focus results in higher collimation.

In simulation model, the LEDs with different width were built individually, and the receiver was placed on the exit surface of parabolic TIR reflector to detect luminance angular profile of reflected light, as shown in Fig. 4-1. The simulation result illustrates that the angular profile varies with value of c/w, as shown in Fig. 4-2. To analyze the result of luminance angular profile quantitatively, full width at half maximum (FWHM) angle is utilized. The relationship between FWHM angle and value of c/w is shown in Fig. 4-3. Higher value of c/w yields lower FWHM angle, which means higher collimation. To deserve to be mentioned, in the ideal point source case, the result of luminance angular profile is an impulse function and the FWHM angle is zero.

Luminous exitance spatial profile which is also affect by stray light is analyzed in the following section.

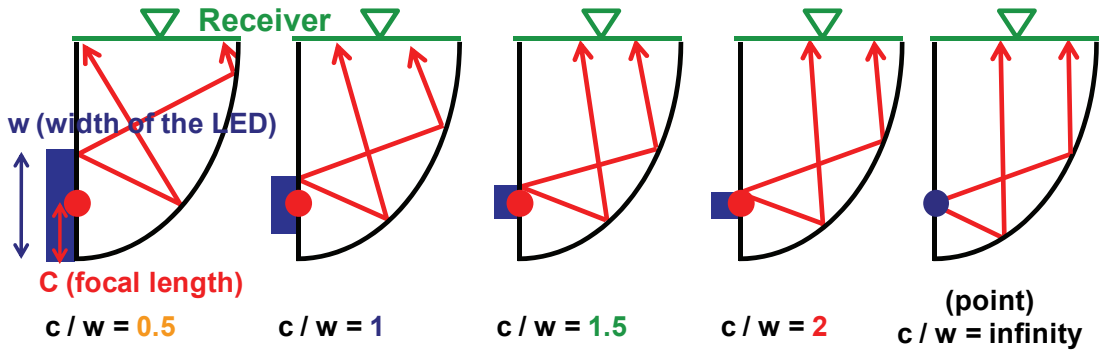

Fig. 4-1 Stray light effect in different c/w and simulation model

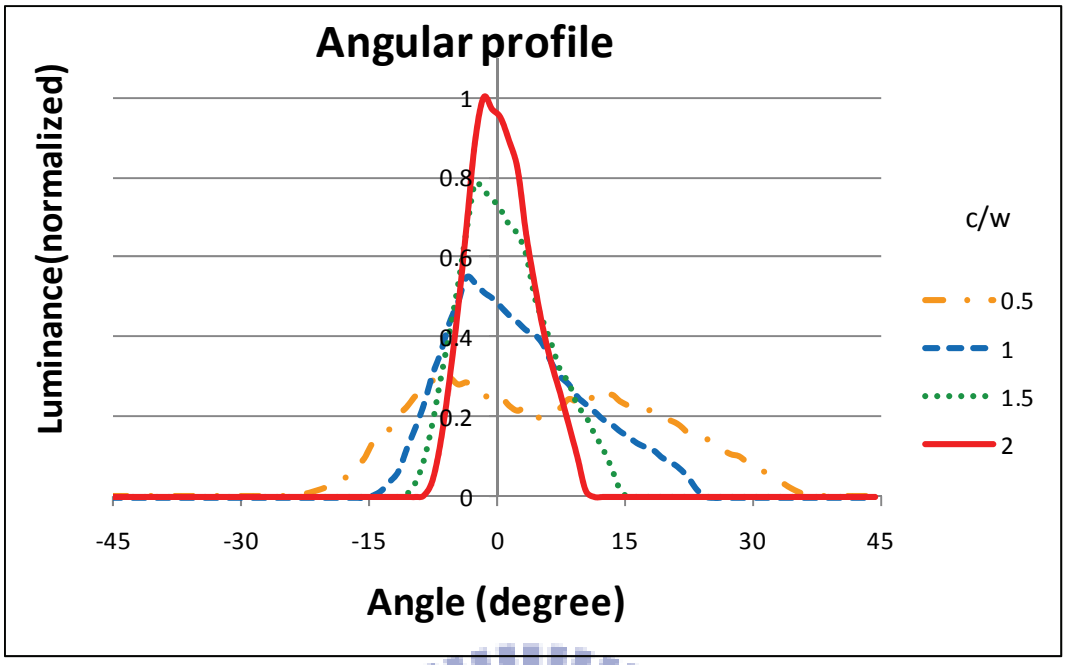

Fig. 4-2 The luminance angular profile with varied c/w

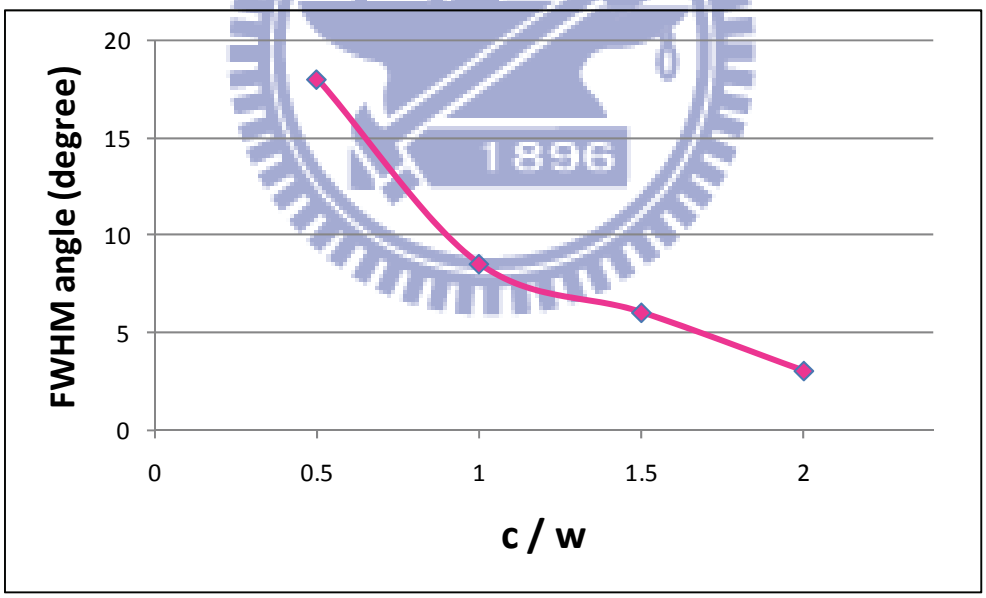

Fig. 4-3 The FWHM angle with varied c/w

4.1.2 **Luminous exitance spatial profile**

The simulation result shows that the LED size more approximative an ideal point source contributes to lower spatial uniformity on the exit surface of the parabolic TIR reflector. In other words, high uniformity is attributed to low value of c/w with the light which is emitted from the points around the LED center.

Fig. 4-4 illustrates the simulation result that the luminous exitance spatial profile varies with value of c/w. The segment is designated to quantify the uniformity. The segment uniformity is defined as minimum luminous exitance divided by maximum luminous exitance in the range of the segment. Lower value of c/w yields higher segment uniformity, as shown in Fig. 4-5.

The relationship between collimation and uniformity is discussed in the following section.

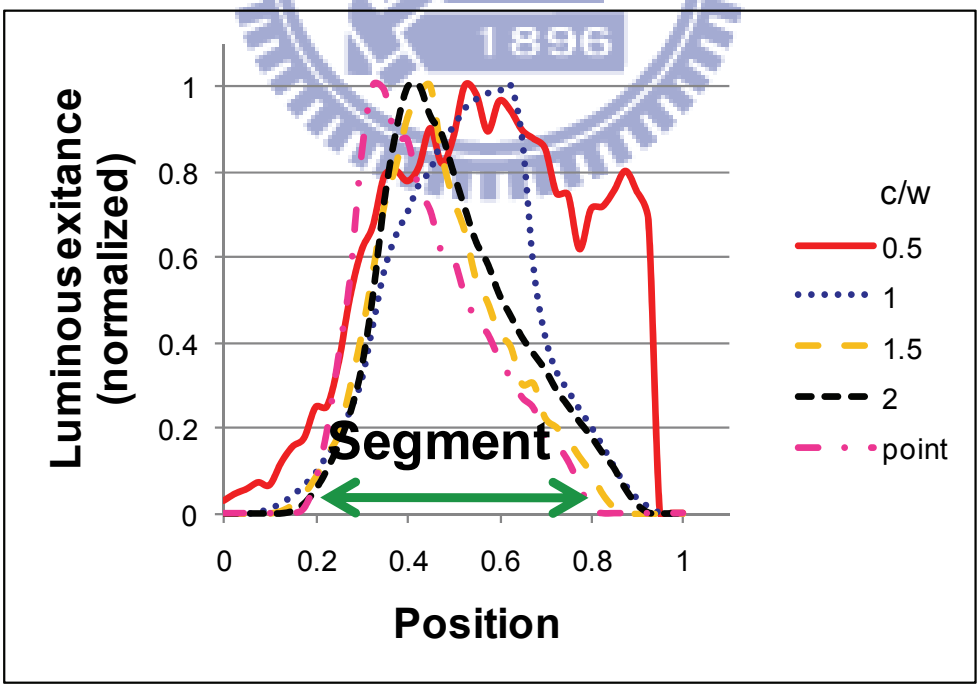

Fig. 4-4 The luminous exitance spatial profile with varied c/w

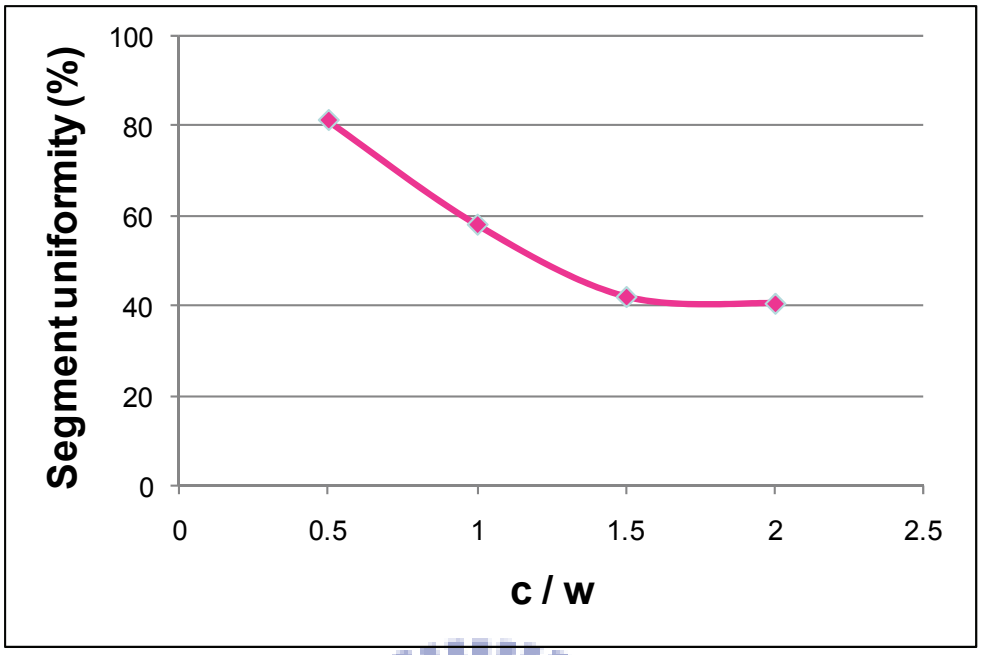

Fig. 4-5 The segment uniformity with varied c/w

4.1.3 **Analysis and Discussion**

Basing on the results of previous two sections, the LED more approximative an ideal point source contributes to higher collimation but lower uniformity. Therefore, it is a trade-off between collimation and uniformity. As the value of c/w is chosen as one, the radiated distribution has narrow divergent angle and keeps relatively high uniformity.

However, the segment uniformity does not represent the completed uniformity of linear light. Fig. 4-6 illustrates the luminance spatial profile with the value of c/w as one. The range where luminance is zero is attributed to the Fresnel loss from parabolic TIR reflector, and it leads to dark zone, as shown in Fig. 4-7. To eliminate the dark zone, the parabolic TIR reflectors are cut off and arrayed continuously, as shown in Fig. 4-8.

The parabolic TIR reflector of light guide can convert point source into collimated and uniform linear light. The out-coupler of light guide which can convert linear light into uniform planar light is described in the next section.

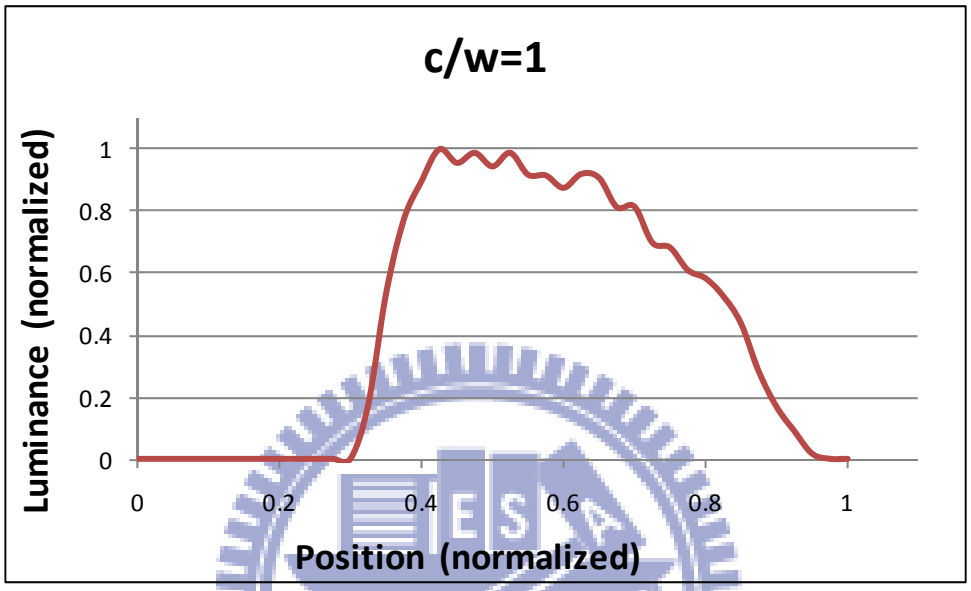

Fig. 4-6 The luminance spatial profile with c/w as one

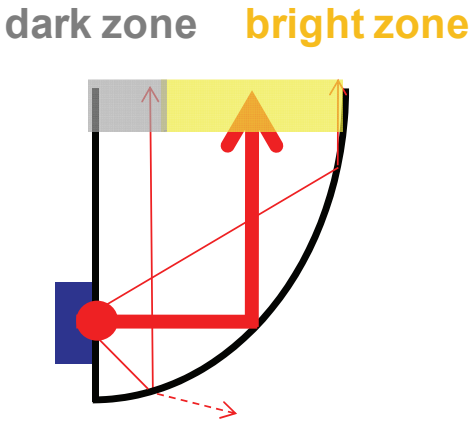

Fig. 4-7 The dark zone attributed to Fresnel loss

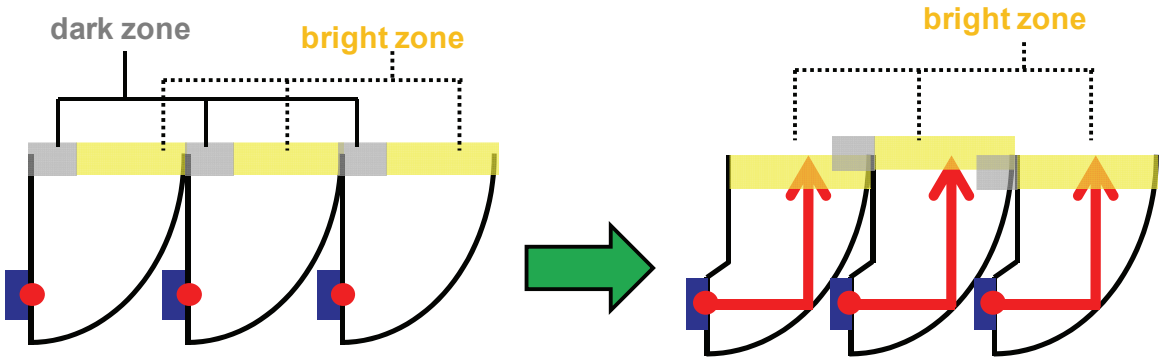

Fig. 4-8 The cut off and arrayed continuously parabolic TIR reflectors for eliminating the dark zone

4.2 Out-coupler

The out-coupler is used to break TIR in light guide, and radiate light out of light guide for luminance angular profile toward the normal of light guide and uniform planar light, as shown in Fig. 4-9[32]. The out-couplers are classified by their working principle, including scattering, diffraction, reflection, refraction, and variable cross-section. Among these types, the v-cut pattern, which combines reflective with refractive, is selected due to the suitability for simulation and fabrication.

The parameters of v-cut array include geometric shape and density distribution, as shown in Fig. 4-10. The geometric shape is optimized for the luminance angular profile toward the normal of light guide, and the density distribution is optimized for uniform planar light in luminous exitance spatial profile. The simulation results of optimization are described in the following section.

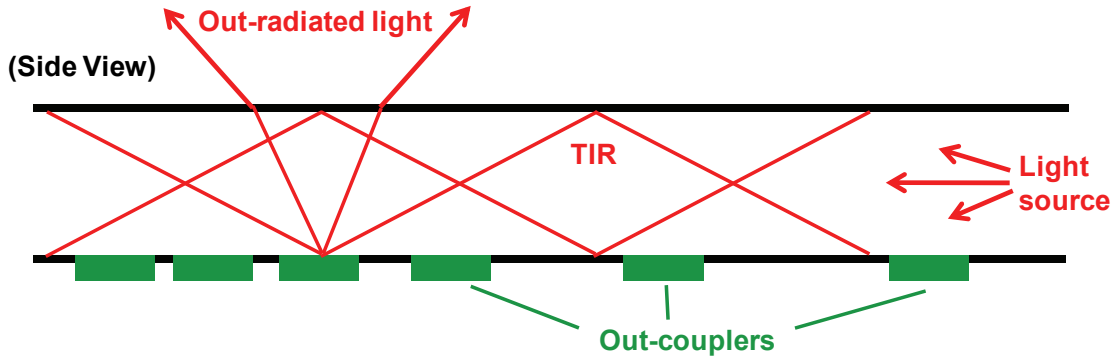

Fig. 4-9 The illustration of out-coupler

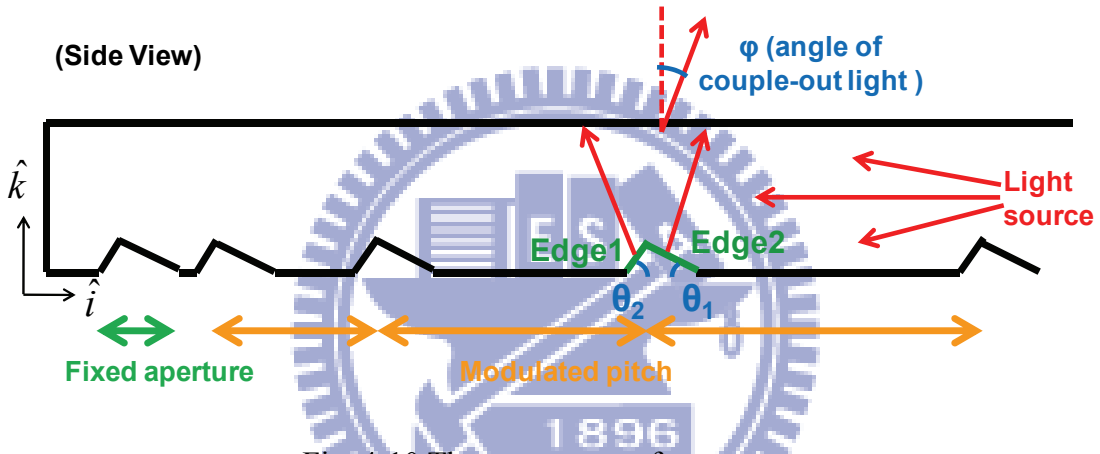

Fig. 4-10 The parameters of v-cut array

4.2.1 **Luminance angular profile**

The angles of v-cut array, θ_1 and θ_2, are optimized for the luminance angular profile toward the normal of light guide, as shown in Fig. 4-10. The simulation result shows that luminance angular profile has dual peaks at φ_1 and φ_2, which are attributed to the occurrence of reflection and refraction at the edge2 simultaneously, as shown in Fig. 4-11. The θ_1 affects the position of φ_1, and the θ_2 effects the value of L_2/L_1, which L_1 and L_2 are the luminance at φ_1 and φ_2.

The luminance angular profile with φ_1 at zero occurs when θ_1 is 55 degrees in

the condition of fixed θ_2, as shown in Fig. 4-12. In the condition which θ_1 is fixed at 55 degrees, the fewest non-on-axis light with lowest L_2/L_1 occurs when θ_2 approach 90 degrees, as shown in Fig. 4-13. However, the top corner of v-cut as at least 60 degrees is suitable for the fabrication of the scrap removing. Therefore, the θ_2 is chosen as 65 degrees.

In additional to the shape of v-cut array, the density distribution of v-cut array for uniform planar light is described in the next section.

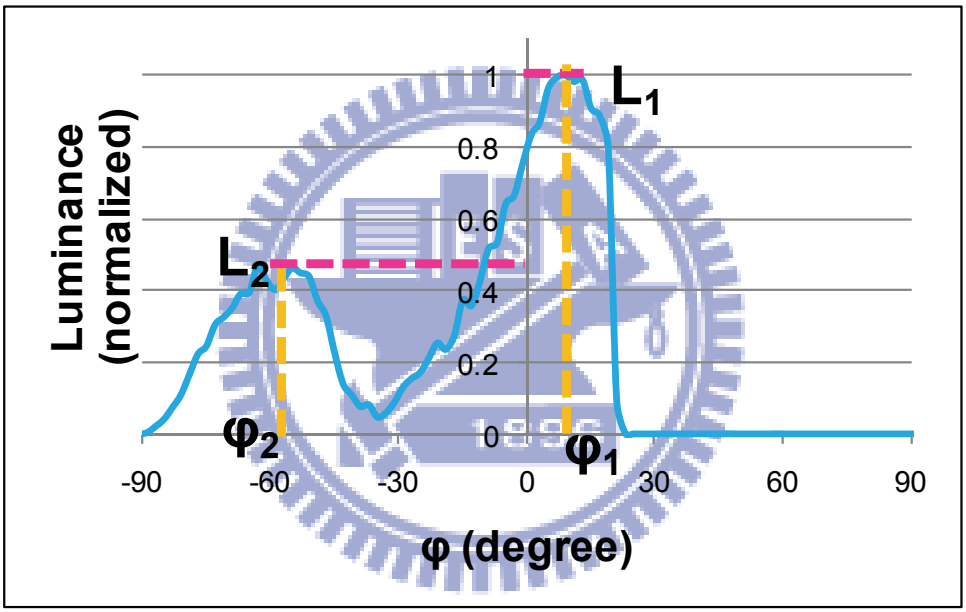

Fig. 4-11 The luminance angular profile

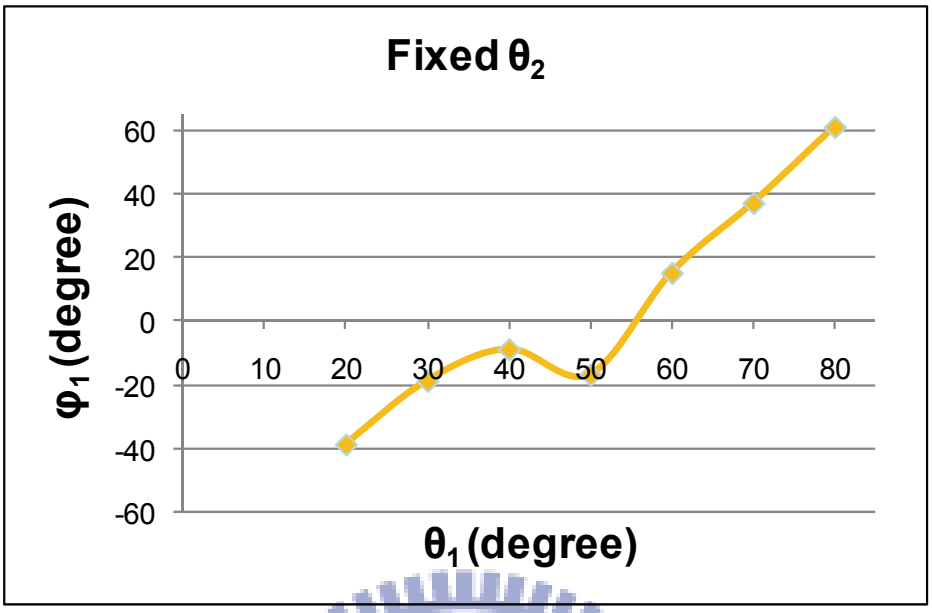

Fig. 4-12 The φ_1 with varied θ_1

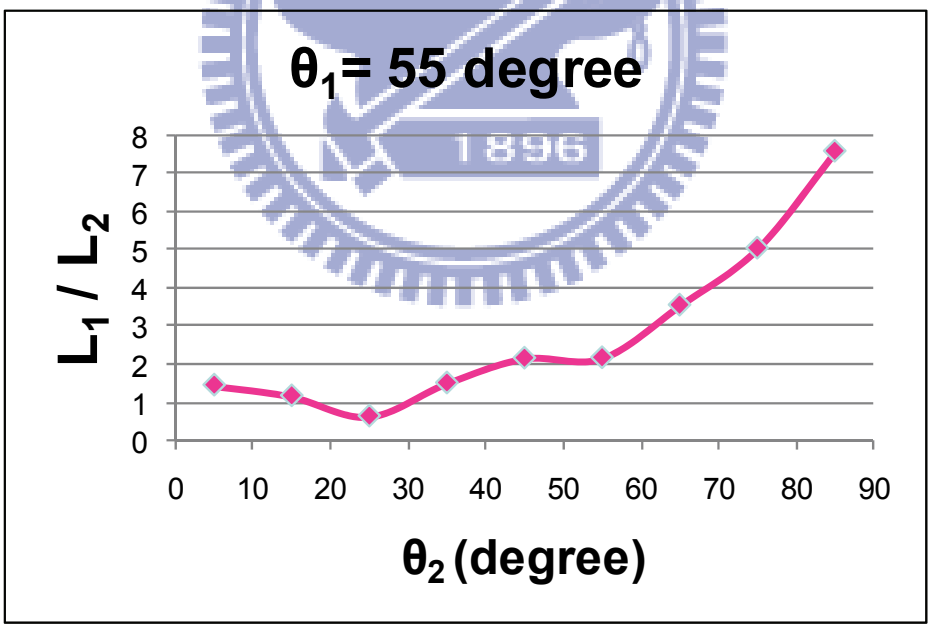

Fig. 4-13 The L_2/L_1 with varied θ_2

4.2.2 **Luminous exitance spatial profile**

The non-uniform density distribution of v-cut array is optimized for uniform planar light in luminous exitance spatial profile. According to the distant from light source, the extraction efficiency in each division varies to reach high uniformity by adjusting the density distribution of v-cut array.

The energy of guided light decays with propagating in light guide. Therefore, the extraction efficiency increases with the distant from light source. The extracting efficiency is found to be positively proportional to the filling factor of v-cut array. The filling factor ascribed to the arrangement density is defined as the fixed aperture of v-cut shape divided by the modulated pitch. Fig. 4-14 illustrates the optimized filling factor distribution, and the simulation result of luminous exitance spatial profile with 88% uniformity is shown in Fig. 4-15.

As the filling factor is optimized, the ratio of v-cut aperture to pitch is fixed. High absolute value of v-cut aperture can reduce the effect on the fabrication error. However, high pitch is easily perceived by human eyes as striped-mura, as shown in fig[33]. Thus, the pitch is limited to below 500 um.

The precise specification of the light guide is described in the next section.

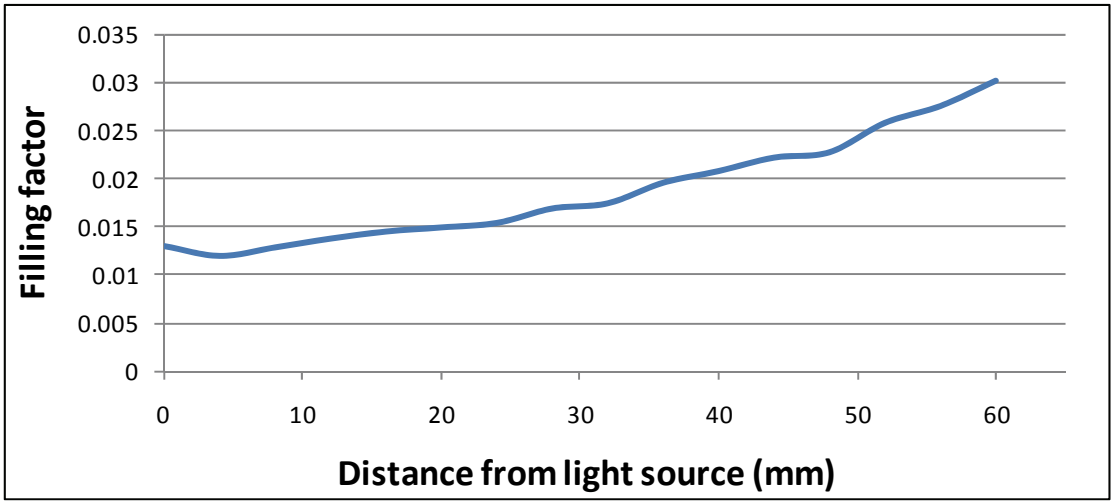

Fig. 4-14 The optimized filling factor distribution

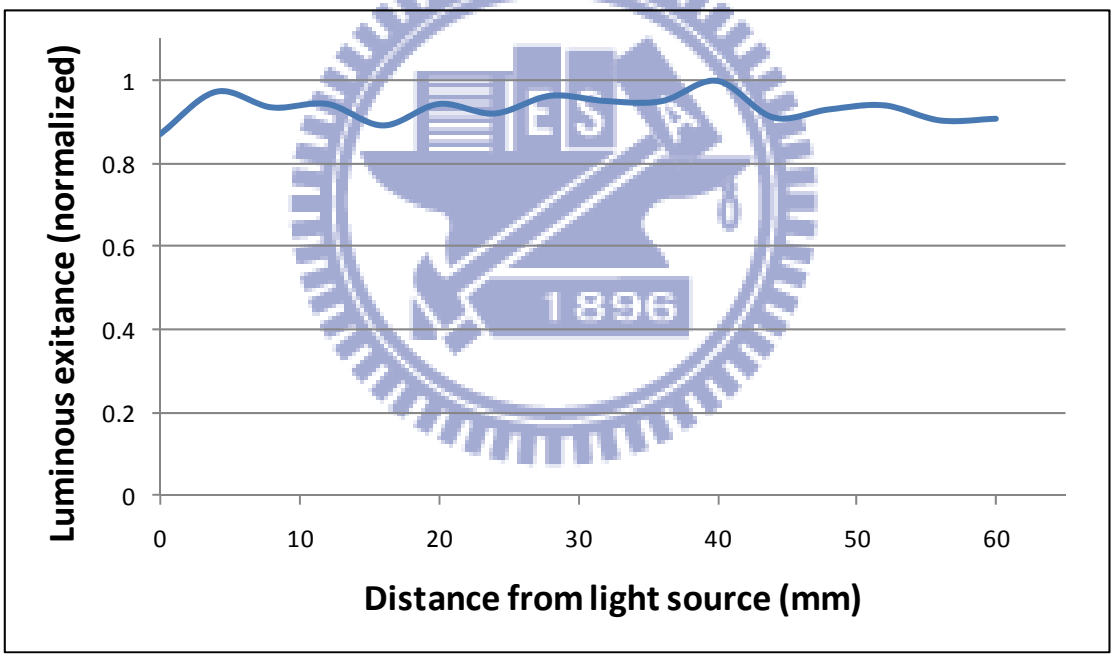

Fig. 4-15 The simulation result of luminous exitance spatial profile with 88% uniformity

Fig. 4-16 The striped-mura

4.3 Summary

The optimized parameters in this chapter are summarized in Fig. 4-17, Fig. 4-18 , Table 4-1, and Table 4-2. In parabolic TIR reflector, the value of c/w as one with the width of LED as 2mm and the focus length of parabola as 2mm is chosen to satisfy the collimation and uniformity simultaneously, with FWHM angle as 8 degrees and segment uniformity as 60%. To eliminate the dark zone, the parabolic TIR reflectors are cut off and arrayed continuously with interval as 6.7mm and depth as 11.8mm. In v-cut part, the θ_1 and θ_2 are selected as 55 and 65 degrees for the luminance angular profile toward the normal of light guide and suitability for fabrication. The modulated filling factor with fixed aperture as 5.8um is optimized for high uniformity and unperceived striped-mura by human eyes.

These optimized parameters are utilized to fabricate the prototype of light guide. The fabrication and experiment are described in the next chapter.

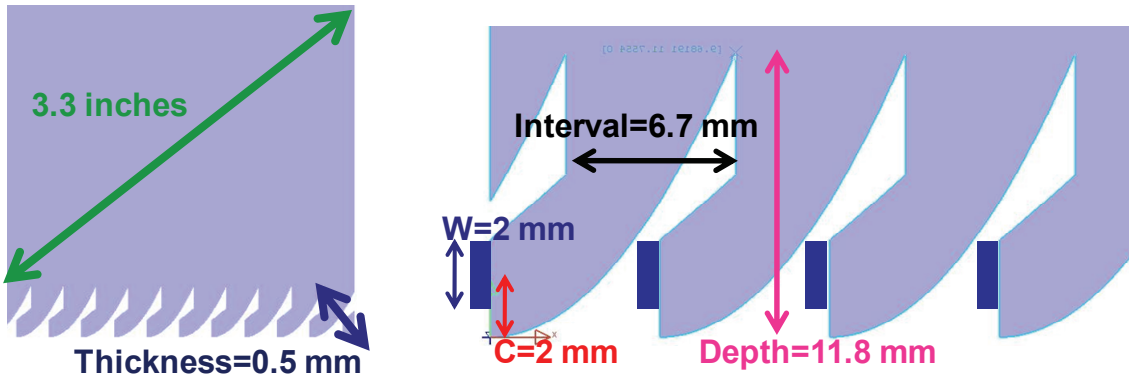

Fig. 4-17 The optimized parameters in parabolic TIR reflector

Parameter	Value
C/W	1
C(focal length)	2mm
W(width of LED)	2mm
Interval	6.7 mm
Depth	11.8 mm

Table 4-1 The optimized parameters in parabolic TIR reflector

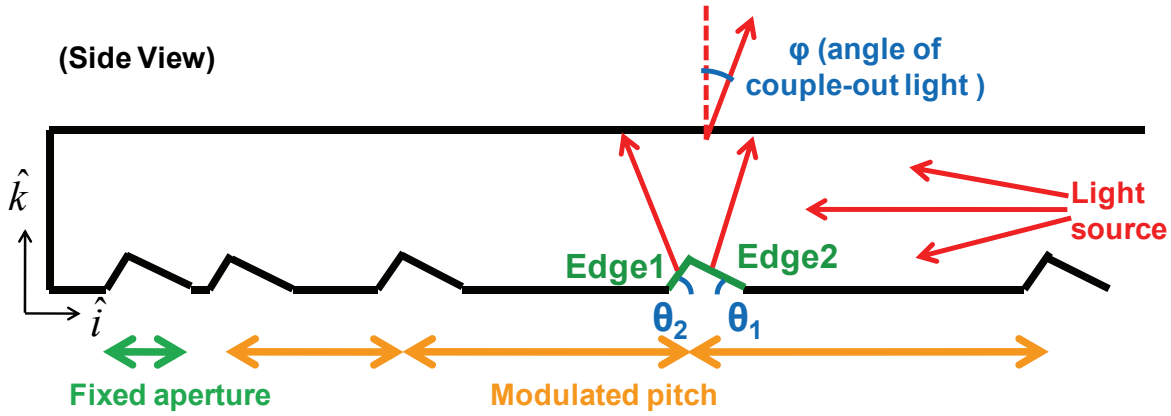

Fig. 4-18 The optimized parameters in v-cut array

Parameter	Value
θ_1	55 degrees
θ_2	65 degrees
Filling factor	0.012~0.03
Aperture	5.8 um

Table 4-2 The optimized parameters in v-cut array

Chapter 5

Fabrication and Experiment

The prototype of light guide was fabricated by the laser micromachining and diamond turning method. To verify the concept of bending-loss prevention, experiment results are discussed as the following section.

5.1 Fabrication technologies and results

The laser cutting was utilized to fabricate the parabolic TIR reflector of light guide[34]. Besides, the v-cut of light guide was fabricated by the diamond turning[35]. Both these two fabrication technologies are provided by ITRI.

5.1.1 Laser cutting

Laser cutting is a technology that uses a laser to cut materials, and is typically used for industrial manufacturing applications, as shown in Fig. 5-1. Laser cutting works by directing the output of a high-power laser at the material to be cut. The material then either melts, burns, vaporizes away, or is blown away by a jet of gas, leaving an edge with a high-quality surface finish. Industrial laser cutters are used to cut flat-sheet material as well as structural and piping materials. Additionally, most industrial lasers have the ability to pulse or cut continuous wave under numerical control program. Now laser cutters have positioning accuracy of 10 um and repeatability of 5 um. Standard roughness increases with the sheet thickness, but decreases with laser power and cutting speed.

The material of light guide is PMMA, because PC and PET will be scorched by laser cutting. When the thickness of PMMA is 0.5 mm, the radius of curvature can not

be lower than 50mm in bending, otherwise it may be broken.

Fig. 5-2 shows that the result of laser cutting is correspond to the designed parabolic TIR reflector.

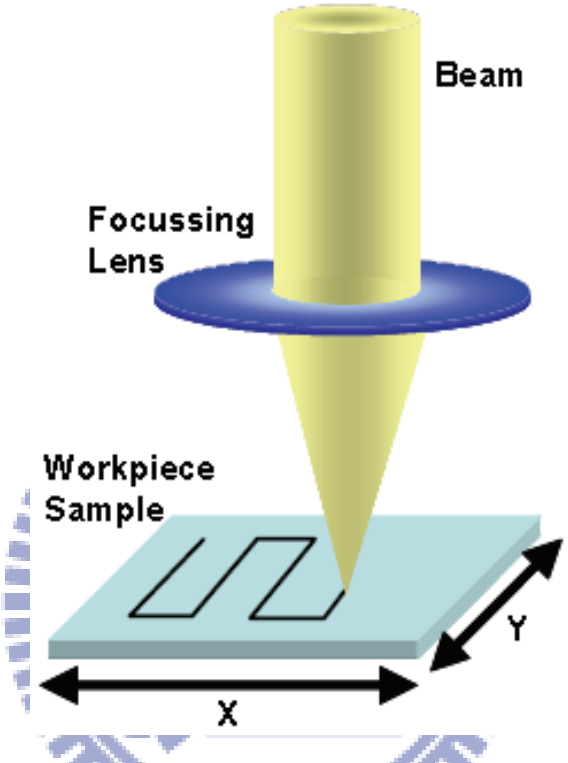

Fig. 5-1 Illustration of laser cutting[36]

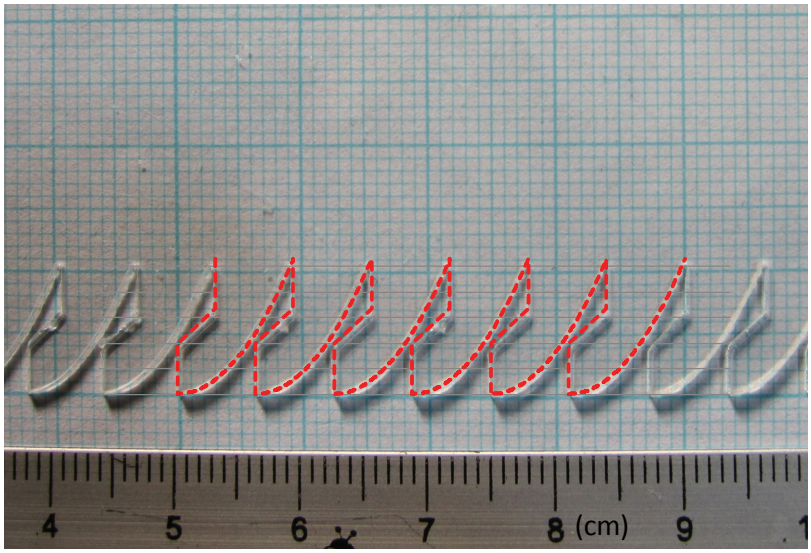

Fig. 5-2 The result of laser cutting

5.1.2 **Diamond turning**

To fabricate the designed v-cut of light guide, the diamond turning was utilized. A single point diamond tool (SPDT) can be used to fabricate a finished optical component on a precision machine under precisely controlled[37]. Although diamond turning application for optical components started in the 1960s, the technology attracted wider attention in the mid-70s. The process step is as the following:

Diamond turning is a multi-stage process. Initial stages of machining are carried out using a series of computer numerical control (CNC) lathes of increasing accuracy. A diamond-tipped lathe tool is used in the final stage of the manufacturing process to achieve a sub-nanometer level surface. The process finishes with sub-micrometer form accuracies. The surface finish quality is measured as the peak-to-valley distance of the grooves left by the lathe. The form accuracy is measured as a mean deviation from the ideal target form. Finally, the quality and accuracy is monitored throughout the manufacturing process using equipment such as laser profilometers, laser interferometers, optical and electron-microscopes.

The best quality natural diamonds are used as a single-point cutting element during the final stage of the machining process. A CNC SPDT rests atop a high quality granite base, which is placed on air suspension on a solid foundation to keep its working surface strictly horizontal, creating a quality micrometer surface. The machine tool components are placed on top of the granite base and can be moved with high degree of accuracy using a high-pressure air cushion or hydraulic suspension. The machine element is attached to an air chuck that is separated from the electric motor which spins it to another air cushion.

The cutting tool is moved with nanometer precision using a combination of electric motor piezoelectric actuators. The motion of the tool is controlled by a list of coordinates generated by a CAD model. The final surface is achieved with a series of decreasing pitch cutting passes.

5.2 Measurement setup

The measurement setups including two parts, according to in flat case or in bending case, are illustrated as below.

When the backlight is in flat case, the measurement setup is shown in Fig. 5-3. The 2D (two dimension) luminance distribution on the backlight was measured by the CCD camera in front of the backlight with 1.5 meter.

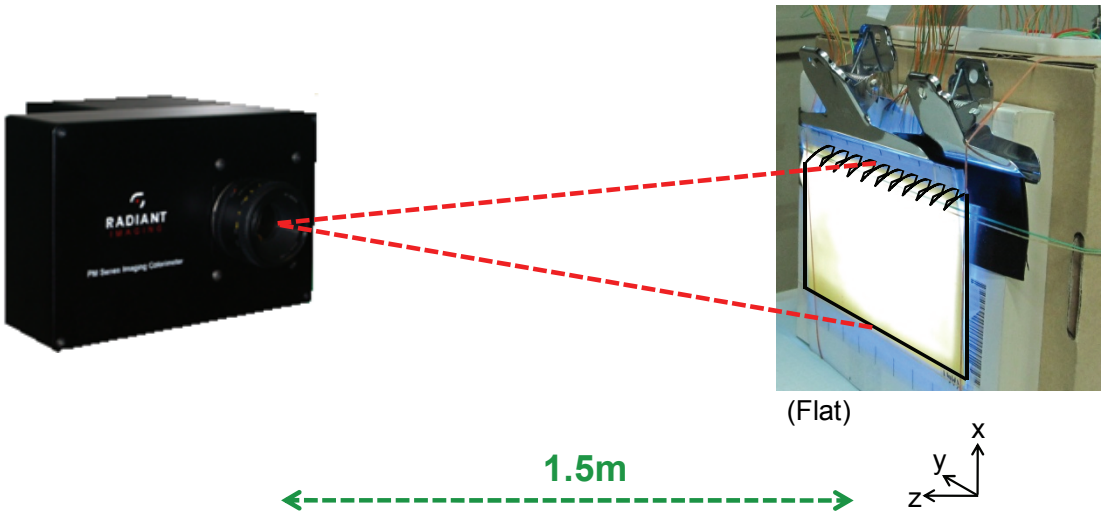

Fig. 5-3 The measurement setup of CCD camera

The measurement setup, which the backlight is in bending case, is illustrated in Fig. 5-4. The luminance of 7x7 points on the backlight, as shown in Fig. 5-5, was measured by the spectro-radiometer from the normal of the backlight. The backlight was bent into different radius of curvature as 150, 100, 70, or 50mm respectively.

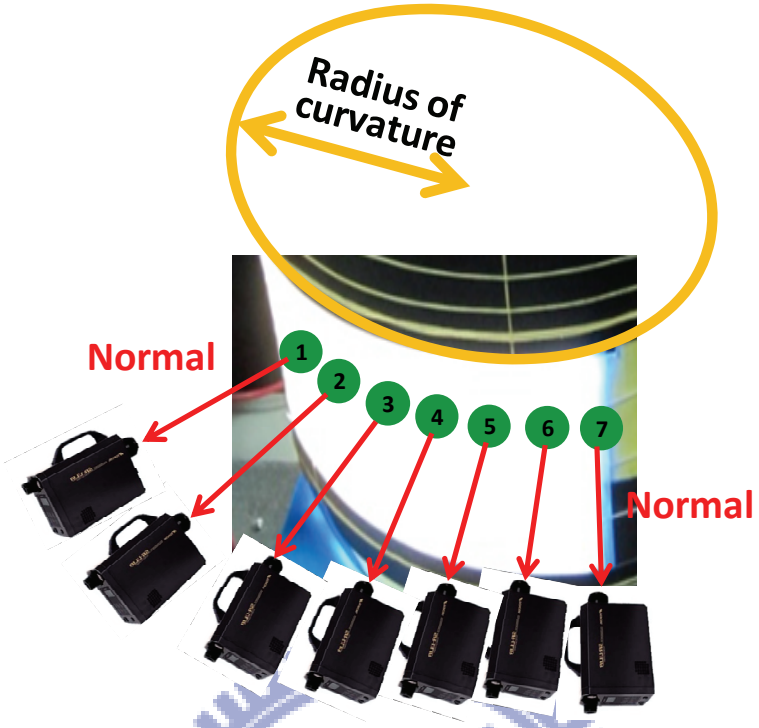

Fig. 5-4 The measurement setup of spectro-radiometer

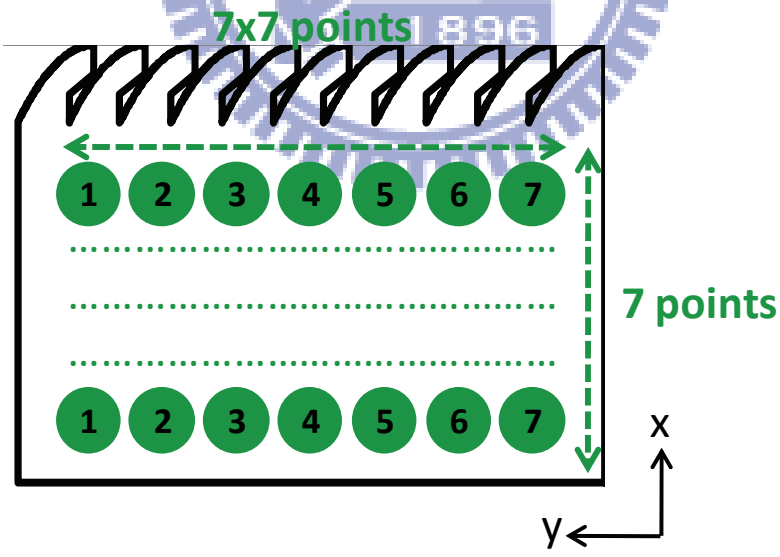

Fig. 5-5 The measurement points on the backlight

5.3 Experimental results and discussions

Light spreading function of unit cell

Light spreading function of unit cell was measured by the CCD camera. In flat case, only a single LED was turned on, as shown in Fig. 5-6. The real image is shown in Fig. 5-7, and the result of 2D luminance distribution is shown in Fig. 5-8. The positions y of maximum and half value are indicated in the fixed x. The points of maximum and half are linked as lines respectively. The divergent angle between two half lines is about 10 degrees. Therefore, the collimated light is successfully obtained by the parabolic TIR reflector as simulation.

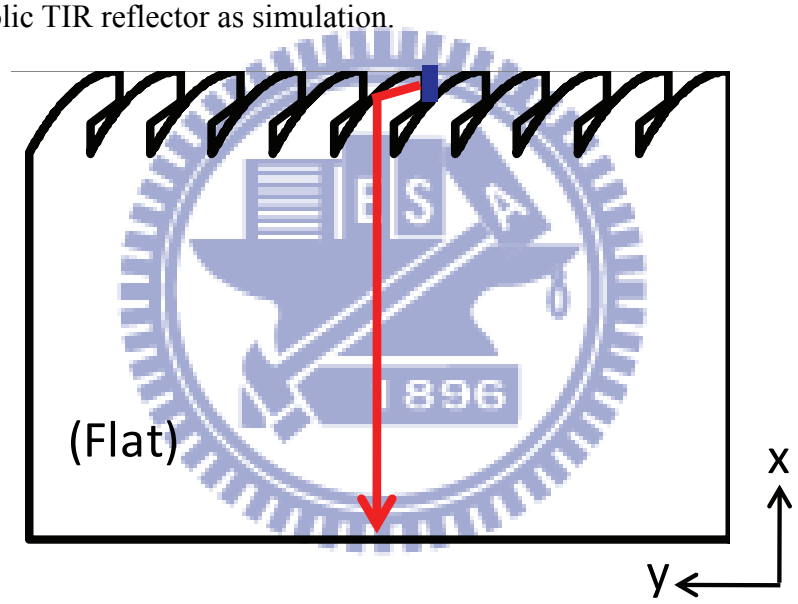

Fig. 5-6 The illustration light spreading function in unit cell

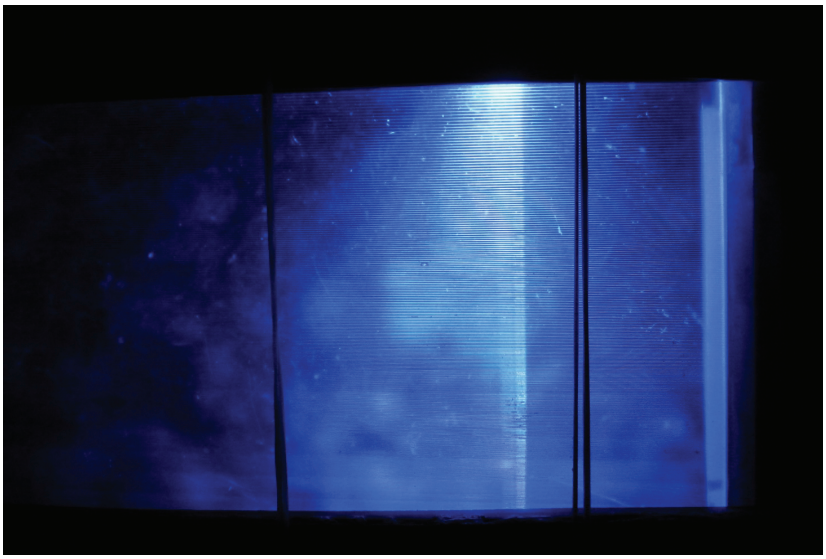

Fig. 5-7 The real image of light spreading function in unit cell

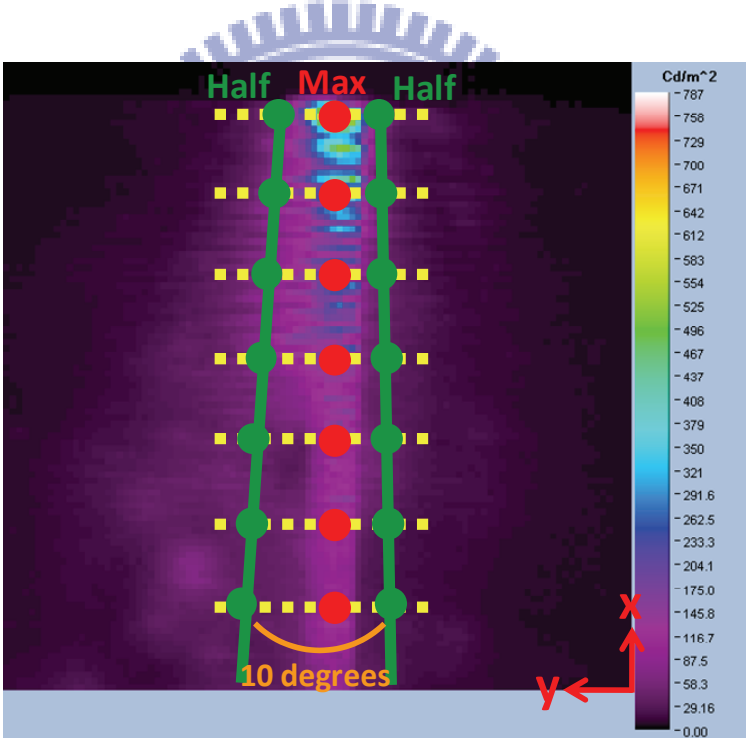

Fig. 5-8 The 2D luminance distribution of light spreading function in unit cell

2D luminance distribution on the whole backlight

And then all the LEDs were turned on. Diffuser and phosphor film were added on the light guide, as shown in Fig. 5-9. The 2D luminance distribution on the whole

backlight was measured by the CCD camera. The real image is shown in Fig. 5-10, and the result of 2D luminance distribution is shown in Fig. 5-11. The 2D uniformity defined as minimum luminance divided by maximum luminance is about 60%. However, the uniformity is so low that human eyes can perceive the difference of brightness. As shown in Fig. 5-12, the difference of brightness comes from the dark and bright regions, which caused by the fabrication error of v-cut. Therefore, to exclude the effect on the defect of v-cut fabrication, and to verify the difference between in flat case and in bending case, the new measurement method and the new definition of uniformity will be illustrated in the following sections.

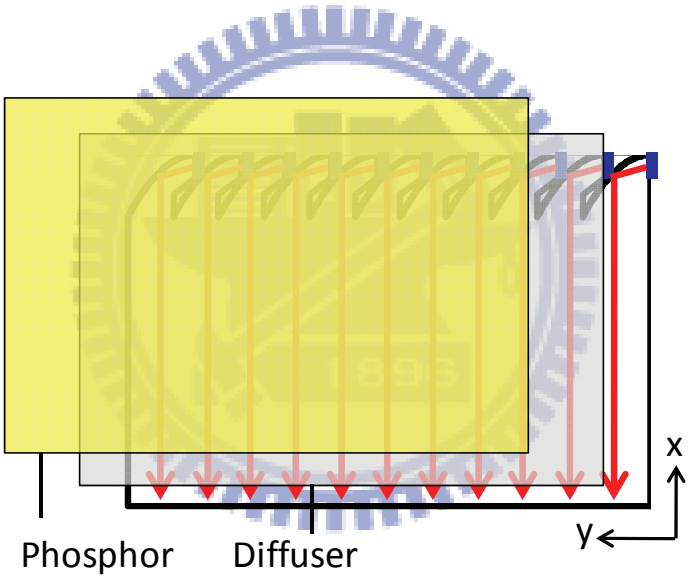

Fig. 5-9 The illustration of 2D luminance distribution on the whole backlight

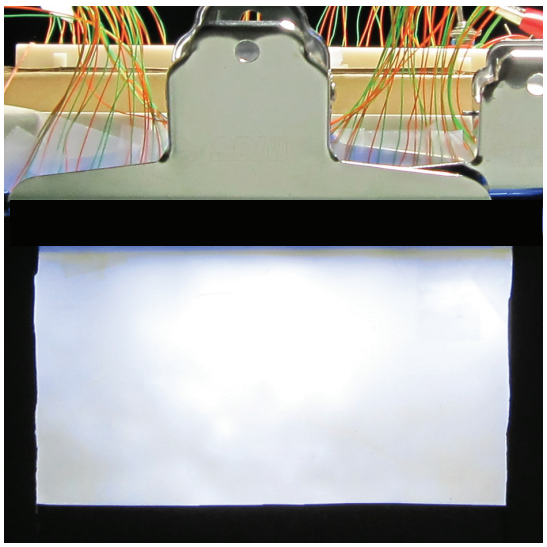

Fig. 5-10 The real image of 2D luminance distribution on the whole backlight

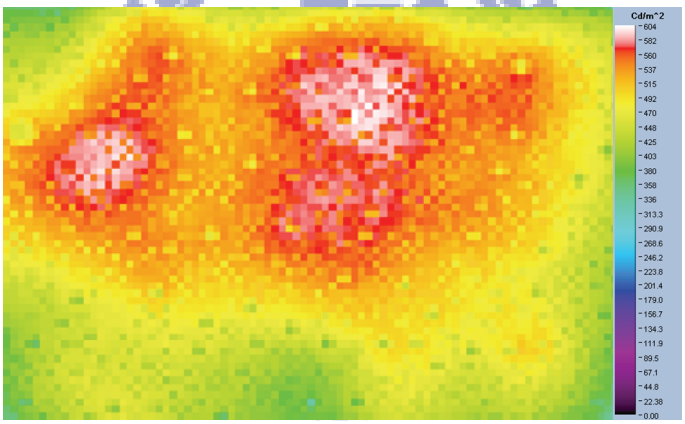

Fig. 5-11 The 2D luminance distribution on the whole backlight

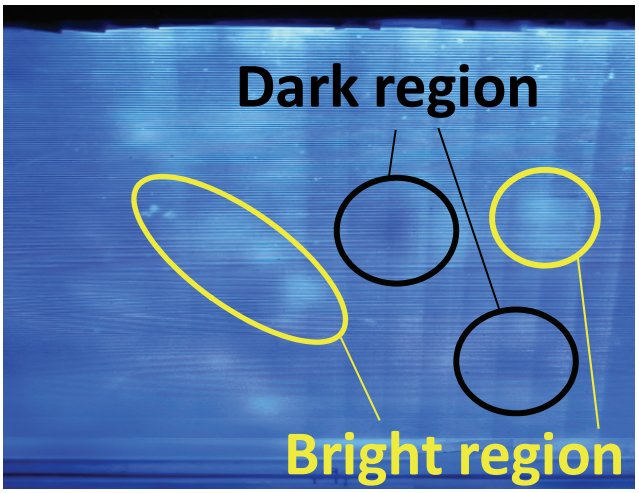

Fig. 5-12 The real image of 2D luminance distribution on the light guide

Average luminance of each row in bending case (1D uniformity)

The luminance of 7x7 points on the backlight was measured by the spectro-radiometer from the normal of the backlight with different bending. The average of luminance in each row is calculated, as shown in Fig. 5-13. Fig. 5-14. illustrates the calculated result, which x-axis represents the position, y-axis means the row average luminance, and the lines are in different bending. The 1D uniformities defined as minimum row average luminance divided by maximum row average luminance are almost higher than 80%, as shown in Fig. 5-15. Therefore, by excluding the effect on defect of v-cut fabrication, the 1D uniformity can be kept in different bending.

Additionally, to verify the difference between in flat case and in bending case, the error function (EF) is defined as the formula below:

$$EF = \frac{\sqrt{\frac{1}{N}\sum_{y=1}^{7}[L_{Bending}(y) - L_{Flat}(y)]^2}}{\overline{L_{Flat}}} \quad (5.1)$$

where N is the amount of the rows, $L_{Bending}$ (y) and L_{Flat} (y) are the average luminance

in the position of row when in bending and in flat. The values of EF are in the range about 5% to 10% with different radius of curvature, and the average value of EF is 7.7%, as shown in Fig. 5-16.

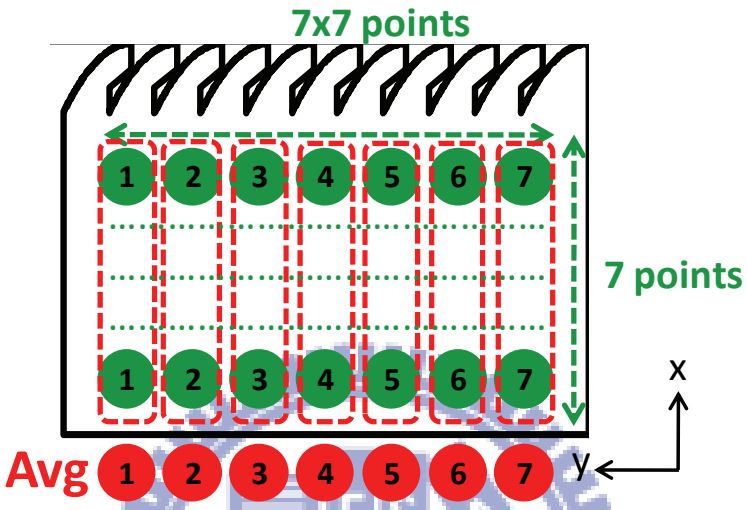

Fig. 5-13 The illustration of average luminance in each row

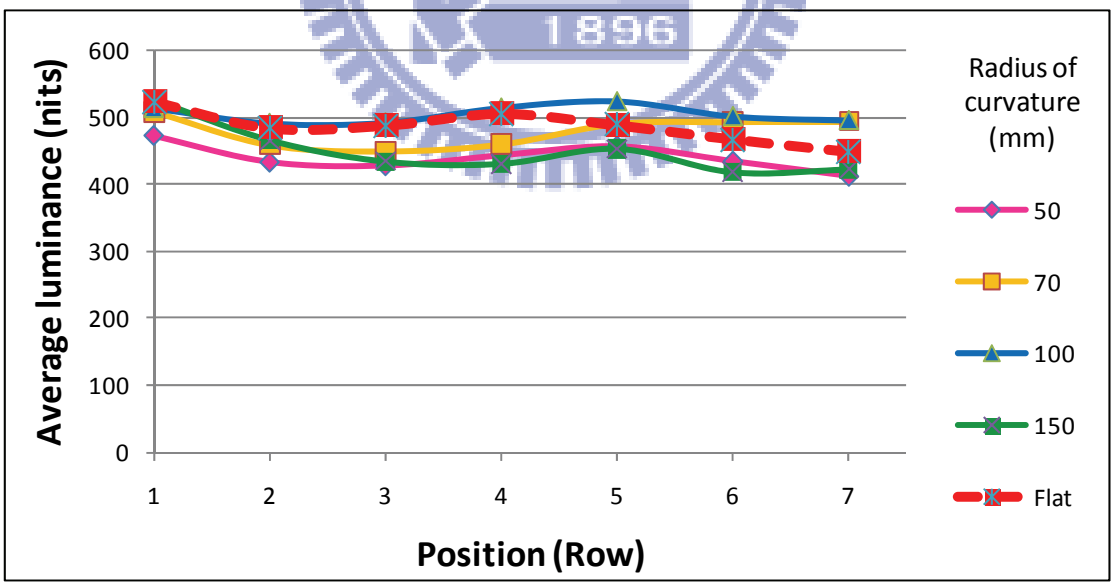

Fig. 5-14 The calculated result of row average luminance with different radius of curvature

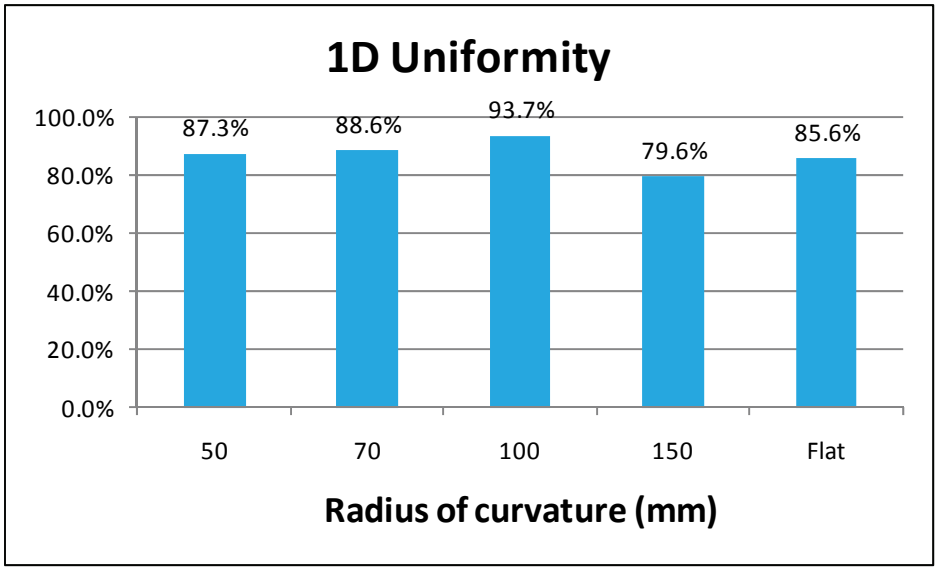

Fig. 5-15 The results of 1D uniformity

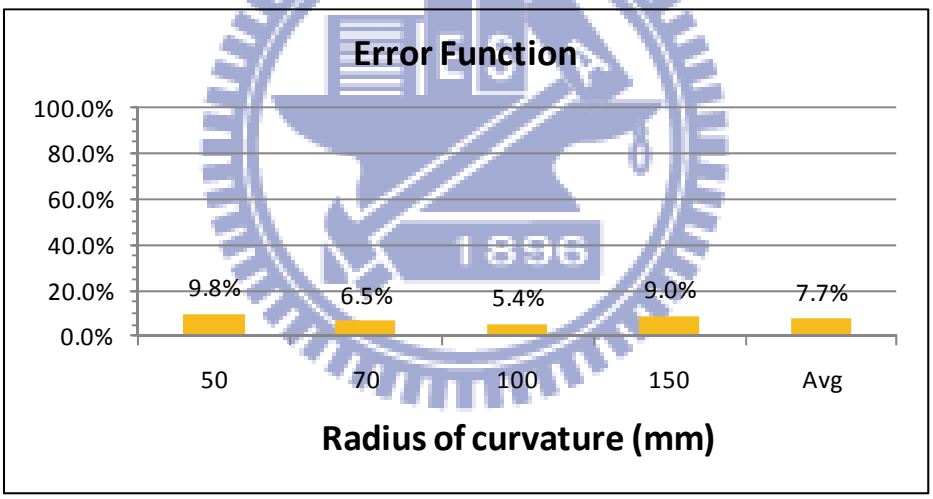

Fig. 5-16 The values of error function

Discussions

However, the value of EF must be zero ideally, which means no difference between in flat case and in bending case. In fact, the difference is attributed to the imperfect collimation, which derived from the experimental result of light spread function in the previous paragraph. The energy flux is 47% in the unit cell, and

otherwise it is 53%, as shown in Fig. 5-17 and Fig. 5-18. The ratio of non-collimated luminous exitance to collimated luminance is about 12.5%, which the luminous exitance is defined as energy flux divided by area. The affected propagating of non-collimated light results in the difference between in flat case and in bending case.

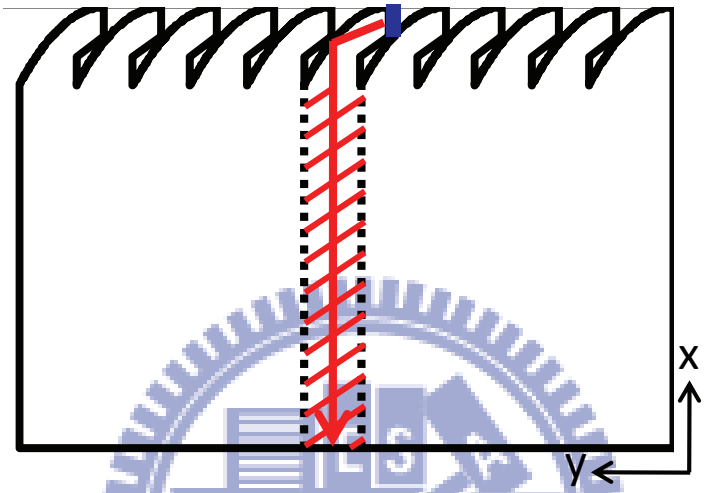

Fig. 5-17 The illustration of energy flux in the unit cell

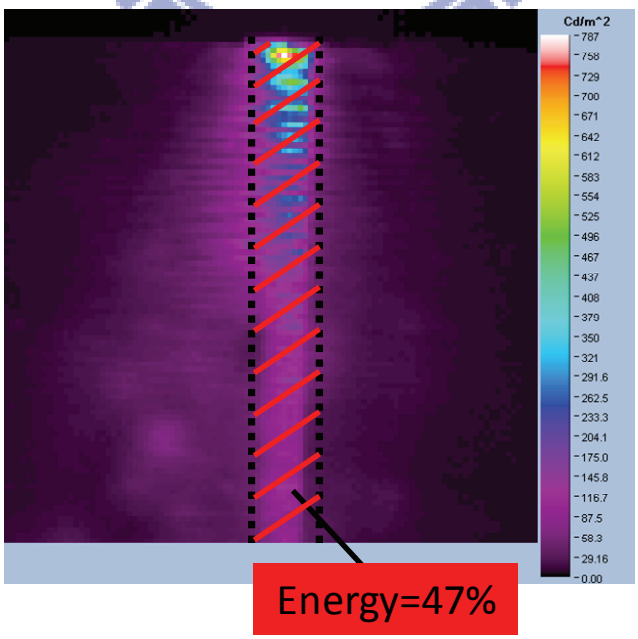

Fig. 5-18 The 2D luminance distribution in the unit cell

Actually, the backlight is not perceived from the normal of the light guide by human eyes. The luminance angular profile of backlight must be considered to correspond with the reality, as shown in Fig. 5-19. The measured result is shown in Fig. 5-20, which the viewing angle is in parallel direction, as illustrated in Fig. 5-21. The luminance angular profile is close to uniform due to the excited Lambertian yellow light from the phosphor. Therefore, the 1D uniformity applied the luminance angular profile (by human eyes) is affected slightly, as shown in Fig. 5-22. The discussion in the previous paragraph is also practicable.

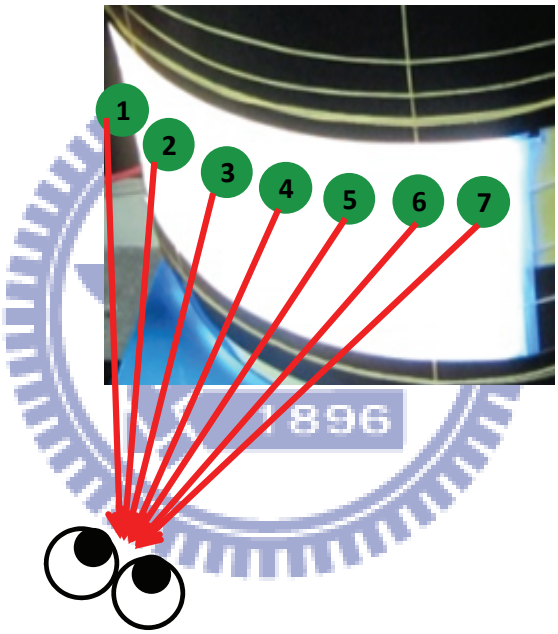

Fig. 5-19 The illustration of observation by human eyes

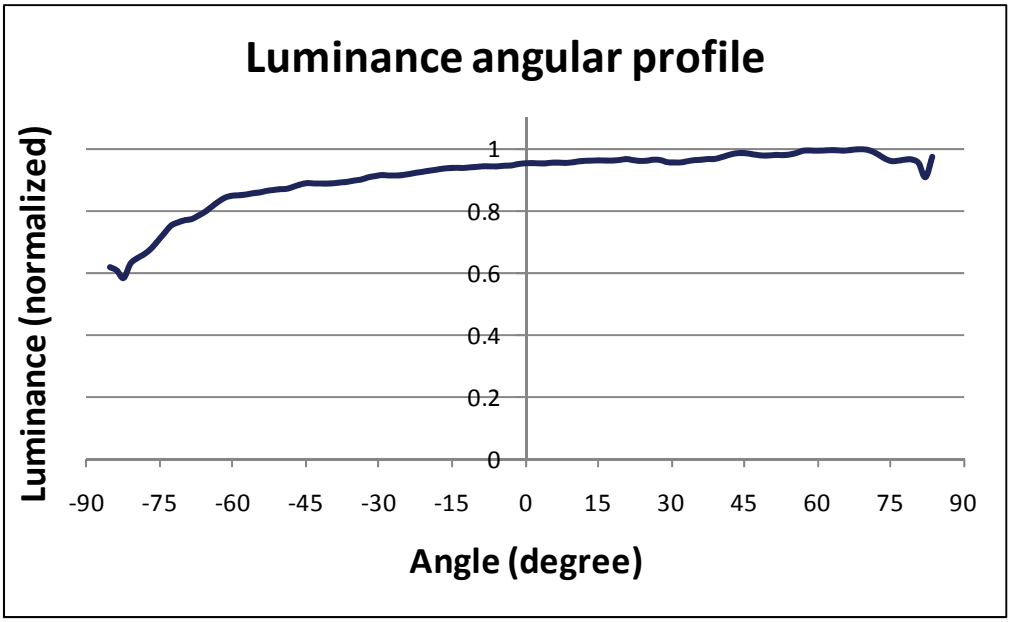

Fig. 5-20 The measured result of luminance angular profile

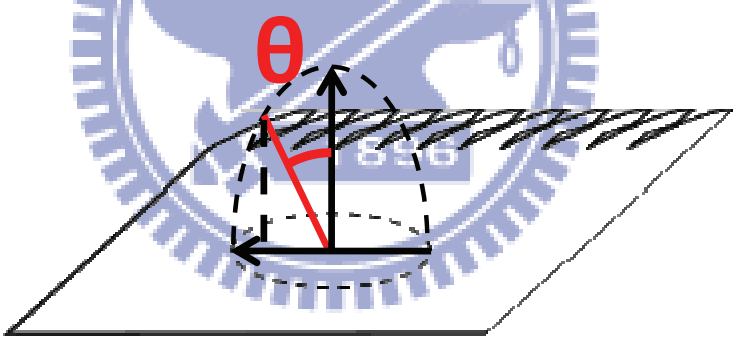

Fig. 5-21 The illustration of viewing angle

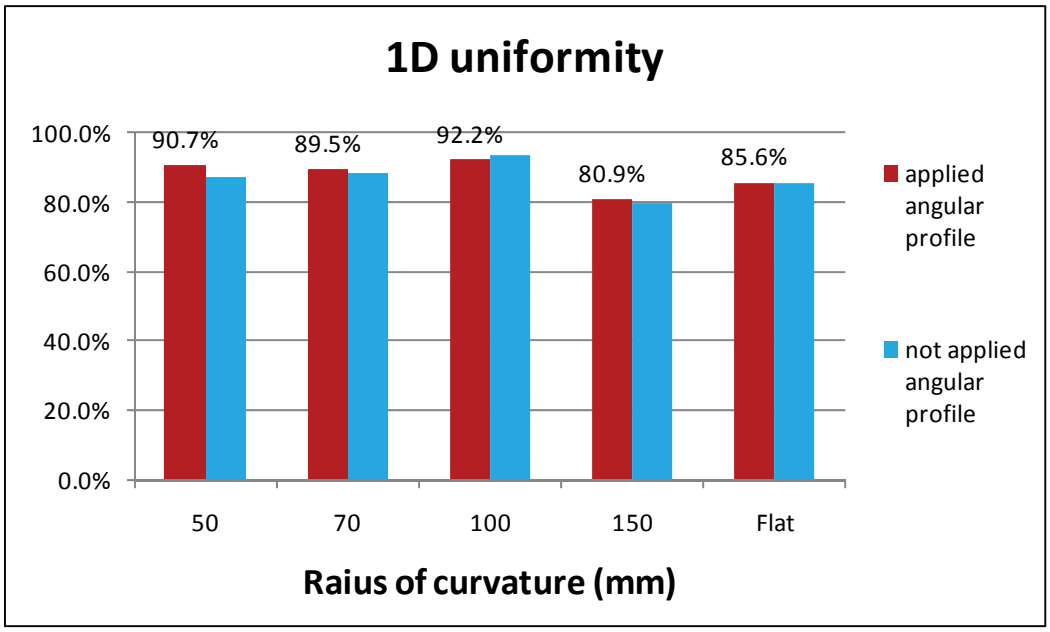

Fig. 5-22 The 1D uniformity before and after applied the luminance angular profile

In micro-observation, the geometric shape of v-cut structure may be affected by bending, which cause the wrinkle. However, the measured luminance angular profiles in different bending are similar, as shown in Fig. 5-23. Additionally, the dark and bright regions from the previous result still exist in flat and bending case. Therefore, the effect on geometric shape of v-cut structure by bending is also slight.

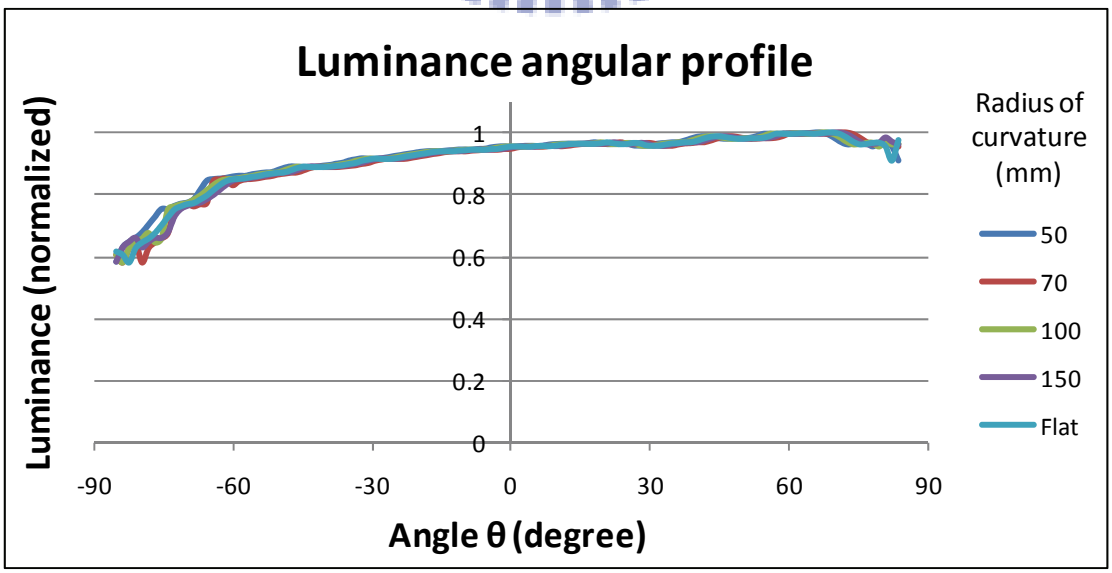

Fig. 5-23 The measured luminance angular profiles in different bending

Chapter 6

Conclusions and Future Work

6.1 Conclusions

In display applications, flexibility will be a trend in the future due to the features like compactness and portability. Flexible displays include OLED, EPD, ECD, and ChLCD. These display technologies suffer different issues. As a mature technology, LCD has the potential for development in flexible display. However, the transmissive LCD requires the backlight for operation. In general, the luminance uniformity of backlight cannot be kept in bending case, which results from the bending-loss.

In this thesis, the flexible backlight with bending-loss prevention was proposed and studied. The parameters, including the parabolic TIR reflector and the v-cut out-coupler, were optimized. Based on the optimized parameters, the prototype of the flexible backlight was fabricated by laser cutting and diamond turning to verify the concept.

From the experimental results, the 2D uniformity in flat case was 60%, and it can be increased by improving fabrication accuracy of v-cut out-coupler on light guide, which will be discussed in the next section. Furthermore, the 1D uniformity with average of each row could be kept over 80% in both bending case and flat case. The EF, which means the difference between in flat case and in bending case, was 7.7%, and it is attributed to the imperfect collimation. Additionally, the 1D uniformity applied the nearly uniform luminance angular profile by human eyes is close to the previous result. Therefore, the flexible backlight with bend-loss prevention has the potential to be applied in flexible LCD.

6.2 Future Work

To improve the fabrication accuracy of v-cut out-coupler on light guide, the two methods below can be applied. The first one is broadening the aperture of v-cut, as shown in Fig. 6-1. The ratio of error to broadened ideal value can be decrease. However, raised pitch may be perceived by human eyes as striped-mura. The second method is the process of micro-injection molding, as shown in Fig. 6-2. It is also suitable for mass production.

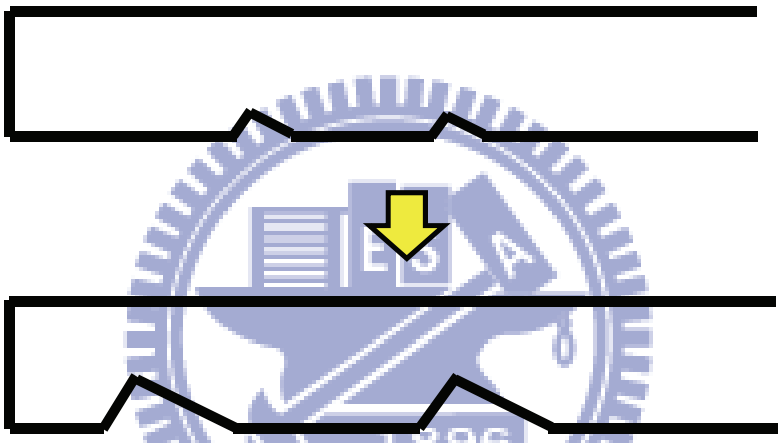

Fig. 6-1 The method with broadening the aperture of v-cut for solving fabrication accuracy

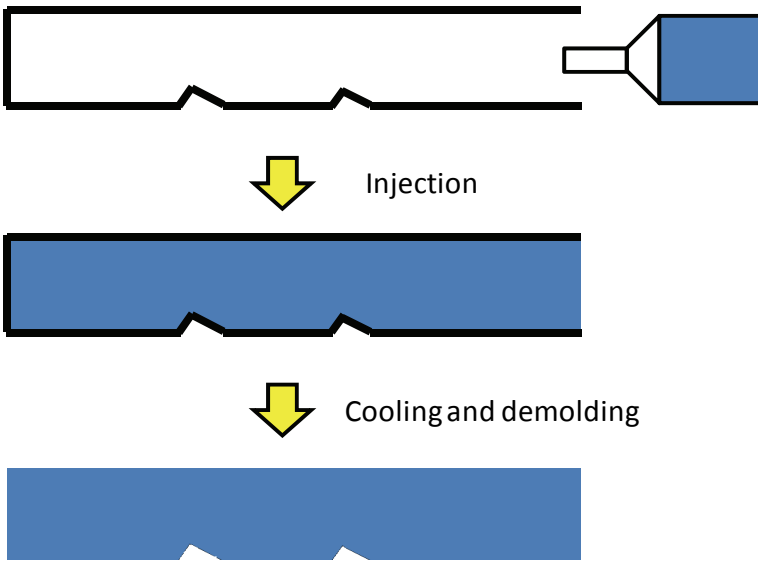

Fig. 6-2 The process of micro-injection molding

Besides, the angular color deviation was not considered in this thesis. It results from the difference of angular profile between diffused blue light and excited yellow light, as shown in Fig. 6-3. To improve the angular color deviation, there are two methods can be applied. The first one is using white LEDs instead of blue LEDs and remote phosphor. Nevertheless, the planar luminance uniformity may be decreased due to the reduced backward scattering of excited yellow light. The 1D uniformity applied luminance angular profile by human eyes will also be decreased because of the directional white light. The second method is adding optimized lenticular films. It can redirect the uniform yellow light toward the normal of light guide, as shown in Fig. 6-4. The measured color difference ($\Delta u'v'$) between different viewing angle (0° and 30°) could be reduced by adding random lenticular films, as shown in Fig. 6-5. Thus, this method was regard as a workable solution.

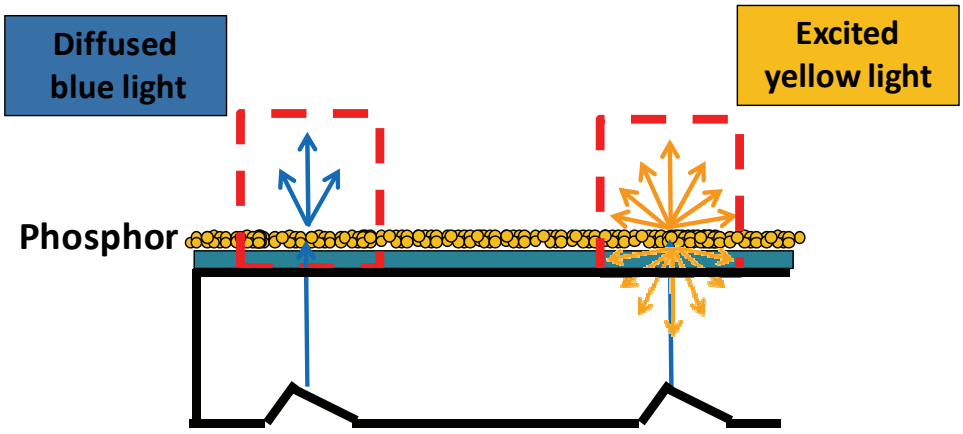

Fig. 6-3 The reason of angular color deviation

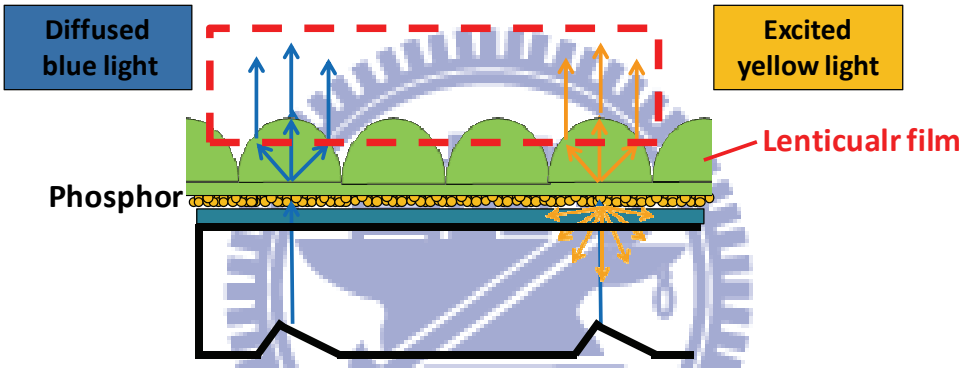

Fig. 6-4 The method with adding optimized lenticular films for solving angular color deviation

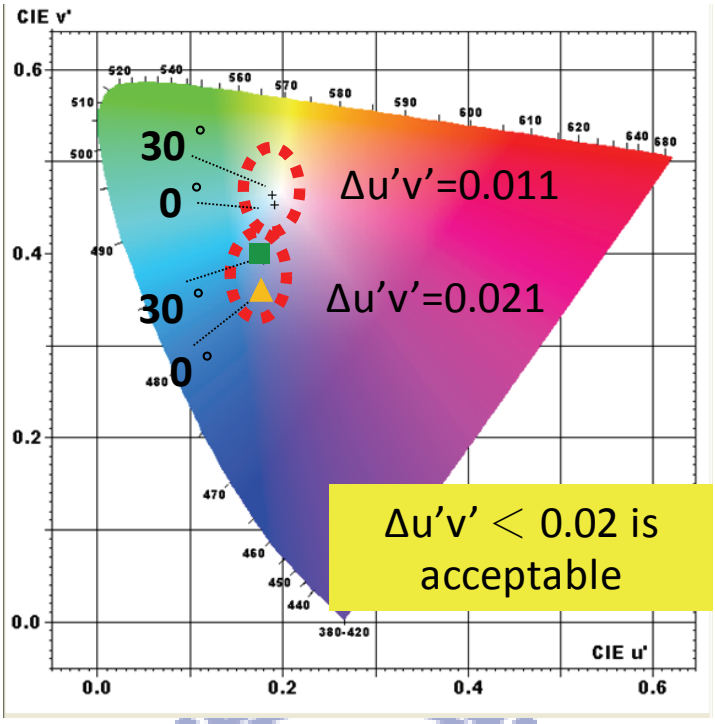

Fig. 6-5 The measured color difference between different viewing angle (0° and 30°) by adding random lenticular films

References

[1] Dawson, R.M.A. et al, “The impact of the transient response of organic light emitting diodes on the design of active matrix OLED displays”, IEDM '98 Technical Digest, pp.875 (1998)

[2] S Nishigaki et al, “Plasma display panel”, US Patent 5,209,688 (1993)

[3] W. B. Choi et al, “Fully sealed, high-brightness carbon-nanotube field-emission display”, Applied Physics Letters, Vol. 75 (1999)

[4] J. I. Pannkove, “Display Devices (Topics in Applied Physics)”, Chap.4, Springer-Verlag (1980)

[5] M. A. Hopper et al, “An Electrophoretic Display, Its Properties, Model, and Addressing”, IEEE transactions on electron devices, Vol. Ed-26 (1979)

[6] Prakash R. Somani et al, "Electrochromic materials and devices: present and future", Materials Chemistry and Physics, Vol. 77, pp. 117-133 (2002)

[7] Gregory P. Crawford et al, "Flexible Flat Panel Displays", Chapter 17, John Wiley & Sons, Ltd (2005)

[8] C. D. Sheraw et al, "Organic thin-film transistor-driven polymer-dispersed liquid crystal displays on fexible polymeric substrates", Applied Physics Letters, Vol. 80 (2002)

[9] N. Narendran et al, “Extracting Phosphor-Scattered Photons to Improve White LED Efficiency, “ Phys. Stat. Sol. (A), Vol. 202 (2005)

[10] H. Luo et al, “Analysis of High-Power Packages for Phosphor-Based White-Light-Emitting Diodes”, Applied Physics Letters, Vol. 86 (2005)

[11] S. C. Allen et al, “EliXIR-Solid-State Luminaire with Enhanced Light Extraction by Internal Reflection”, Journal of Display Tech., Vol. 3 (2007).

[12] S. C. Allen et al, “A Nearly Ideal Phosphor-converted White Light-emitting Diode”, Applied Physics Letters, Vol. 92 (2008).

[13] H.-T. Huang et al, “UV Excited Flat Lighting (UFL) System for LCD-TV Backlight Application”, SID’08 Digest (2008)

[14] B.-W. Xiao et al, “LEDs-based Flat Lighting Device for LCD Backlight Applications”, OPT’08, Sat-S23-01 (2008)

[15] B.-W. Xiao et al, “Optical Simulation and Analysis of Visible-light Excited Phosphor Sheet (VEPS) System”, IDMC ‘09, Wed-P5-01 (2009)

[16] B.-W. Xiao, et al “Optical Properties of Visible-light Excited Phosphor Sheet (VEPS) System”, SID’09 Digest (2009)

[17] D. Hreniak et al, “Synthesis and Optical Properties of Nd3+ doped Y3Al5O12 Nanoceramics”, Journal of Alloys and Compounds, Vol. 341 (2002)

[18] Ian Lee, "Super-Thin Flexible Backlight Module with Taper Structure", Master thesis, NTHU (2008)

[19] Cheng-Chuang Chia et al, "Design of flexible backlight module", OPT (2006)

[20] Bahaa E. A. Saleh et al, "Fundamentals of Photonics", John Wiley & Sons, Inc, pp.4 (1991)

[21] Andreas Timinger et al. “Designing Tailored Free-Form Surfaces for General Illumination”, Proc. of SPIE, Vol. 5186, pp. 128-132 (2003)

[22] Frank J. Pedrotti et al, "Introduction to Optics", Prentice Hall, pp.10-15 (1992)

[23] T. Smith et al, “The C.I.E. Colorimetric Standards and Their Use”, Transactions of the Optical Society, Vol. 33, pp. 73-134 (1931)

[24] R. W. Hunt, “Measuring Colour”, 3rd Edition, Fountain Press, England, pp. 39-57 (1998)

[25] A. C. Harris et al, “Objective Evaluation of Colour Variation in the Sand-burrowing Beetle Chaerodes Trachyscelides White by Instrumental Determination of CIELAB Values”, Journal of the Royal Society of New Zealand, Vol. 20 (1990)

[26] N. Ohta et al, “Colorimetry: Fundamentals and Applications”, John Wiley & Sons, pp.76 (2005)

[27] N. Ohta et al, “Colorimetry: Fundamentals and Applications”, John Wiley & Sons, pp.115 (2005)

[28] N. Ohta et al, “Colorimetry: Fundamentals and Applications”, John Wiley & Sons, pp.119 (2005)

[29] M. D. Fairchild, “Color Appearance Models, Reading, Massachusetts”, Addison-Wesley (1998)

[30] D. H. Alman, et al, “Performance Testing of Color Difference Metrics Using a Color-Tolerance Dataset”, Color Research and Application, Vol. 21, pp.174-188 (1989)

[31] J. Schanda, “Colorimetry: Understanding the CIE System”, Wiley Interscience, pp. 61-64 (2007)

[32] Juan Manuel Teijido, “Conception and design of illumination light pipes”, Université de Neuchâtel Institut de microtechnique (1999)

[33] B.W. Xiao, "Development of Thin Format Light-Excited Flat Lighting Systems for LCD Applications", Master thesis, NCTU (2009)

[34] Henning Klank et al, "CO2-laser micromachining and back-end processing for rapid production of PMMA-based microfluidic systems", Lab Chip, pp.242-246 (2002)

[35] T. Nakasuji et al, “Diamond Turning of Brittle Materials for Optical Components”, CIRP Annals - Manufacturing Technology, Vol. 39, Pages 89-92(1990)

[36] Andrew D. Goater et al, "Laser micromachining of optical biochips", Proceedings of SPIE (2007)

[37] F. Z. Fang et al, "Micro machining of optical glasses." Sadhana, Vol. 28, part 5, pp. 945 (2003)